REVIEW

It's a two-way street: Photoswitching and reversible changes of the protein matrix in photoswitchable fluorescent proteins and bacteriophytochromes

Elsa C. Rodrigues and Andre C. Stiel ®

Institute of Biological and Medical Imaging, Helmholtz Zentrum München, Neuherberg, Germany

Correspondence

A. C. Stiel, Institute of Biological and Medical Imaging, Helmholtz Zentrum München, Neuherberg, Germany
Tel: +49 (0) 89 3187 3972
E-mail: andre.stiel@helmholtz-muenchen.de

Chromophore-bearing proteins that are (reversibly) altered after light illumination are major functional components of nature. They gained considerable attention in the last decades since the dynamic interactions of the chromophore and protein matrix can be used to control downstream effects altering the functionality of proteins, cells, or complete organisms with light (optogenetics). Additionally, the photophysical effects can be employed to add capabilities to optical imaging. For example, light can be used to reversibly switch the signal on or off (e.g., fluorescence). In this article, we review chromophore and protein matrix interactions, focusing on photoswitching fluorescent proteins of the GFP family (RSFPs) and natively photoswitching bacteriophytochromes (BphPs). This review aims to provide an in-depth understanding of the dynamic interplay between photoswitching photophysics and the protein matrix and a thorough discussion on how this connection has been harnessed for the development of optogenetic and imaging tools.

Keywords: bacteriophytochromes; optical imaging; optogenetics; photophysics; protein engineering; reversibly switchable fluorescent proteins; structural studies

Proteins that interact with visible light are involved in numerous key mechanisms of nature, for example, visual phototransduction, light energy harvesting, or light-controlled genetic programs, thus stimulating fundamental biology research. Beyond that, such proteins are essential tools for life science research to study cells or complete organisms without perturbation *in vivo* due to the genetic codability of proteins and the noninvasive nature of light interaction. Applications for light-interacting proteins can be loosely grouped into two categories depending on how the light is used: (a) as an input to trigger a downstream effect or (b) as a readout to visualize localizations or processes in the cell or organism. The key for application in both categories is a highly tunable interplay between the light-absorbing chromophore and the surrounding protein matrix.

Applications in which light triggers a downstream effect are often summarized under the field of optogenetics [1,2]. For instance, light-activated ion channels with rhodopsin chromophores [3] (channelrhodopsins), initially found to be responsible for phototactic reactions of algae, are now a key tool for neurophysiological research where they can be used to achieve

temporally and spatially precise depolarization of neurons [4]. Besides such repurposing of native light response mechanisms, a number of optogenetic tools rely on harnessing photochemical structural changes (*cis*/*trans* isomerization, covalent modification, etc.) of the protein matrix to trigger downstream effects facilitated by non-native effector moieties. For example, protein–protein or protein–second messenger interactions can be activated by light to control cellular pathways [5]. In all cases, light is absorbed by a chromophore resulting in its (transient) photochemical change, which is generally relayed by massive structural changes to the protein matrix, resulting in downstream effects (Fig. 1A).

The second field where light-interacting proteins are widely applied is imaging. The most prominent class is that of fluorescent proteins (FPs), with its historic progenitor being the green fluorescent protein (GFP) [6]. Other classes of proteins used in imaging include phytochromes and phycobiliproteins, which allow access to the near-infrared (NIR) realm [7] or light-oxygen-voltage sensing domains for anaerobic studies [8]. The chromophores of some proteins exhibit (transient) photochemical changes that can be exploited for imaging applications, such as photoswitching (Fig. 1B), photoactivation, or photoconversion. These proteins are prominently used in a multitude of super-resolution fluorescence microscopy techniques, for example, revealing sub-diffraction resolution composition of the cell [9] or protein-complex architecture [10]. In addition, these proteins are also used for (reversible) highlighting [11,12] or background suppression through locked-in detection of the photo-modulated sample signal [13,14]. Although photochemical changes in these proteins can lead to rearrangements of the protein matrix, these changes are often subtle and are generally not the focus of research when looking into their applications.

Initially, FPs were primarily used to report on promoter activity or visualize cellular structures, but their use in the construction of sensors, for example to detect an analyte of interest, quickly became prominent. Commonly, an upstream change to the protein matrix through analyte binding is relayed to the residues near the chromophore, which alters its photophysical properties (Fig. 1C). Lately, an expansion on this approach led to sensors showing additional photo-processes (photoconversion or photoswitching) in the analyte-bound state. In those cases, upstream changes to the protein matrix alter the immediate chromophore surroundings in such a way as to permit the additional photo-processes (Fig. 1D).

In this review, we will explore interactions of the protein matrix and chromophore with an emphasis on reversibly switchable chromophore transitions. We restrict ourselves to two families of photoswitching proteins: reversibly switchable FPs of the GFP-family (RSFPs) and far-red (>~ 630 nm) absorbing bacterio-phytochromes (BphPs). This choice is governed by personal interest and the fact that BphP derivates recently gained considerable interest in the optical imaging field, expanding the range of applicable wavelengths (WL) toward the NIR. More importantly, these two protein families are photoswitchable, yet the interactions of their chromophores with the protein matrix are very different and will be discussed thoroughly in this review. Briefly, RSFPs utilize the matrix of the quasi-inert β-barrel fold as a means to tune the photophysics of the chromophore for the imaging application, with larger matrix rearrangements being rare. By contrast, BphPs are multidomain proteins, which undergo massive structural changes upon photoswitching.

Despite the differences, both classes spark similar ideas regarding imaging, sensor engineering, and optogenetic approaches. We will begin with an overview of the 'native' photoswitching functionality in both classes which is mainly based on structural studies. Then we will move to application concepts harnessing the interactions between the photoswitching chromophore and protein matrix.

Reversibly photoswitching proteins of the GFP family

Reversibly switchable fluorescent proteins are members of the family of GFP-like FPs. FPs revolutionized fluorescence imaging with their autocatalytically formed chromophores enclosed in a versatile-yet-shielding 11-stranded β-barrel (Fig. 2A,B). In RSFPs, two distinct WL control the reversible photoswitching between a fluorescent ON- and nonfluorescent OFF-state, with one of these WL also commonly exciting fluorescence. RSFPs gained attention due to their use in fluorescence super-resolution imaging approaches, wherein the switching can be used to confine fluorescence emission to sub-diffraction sized spots (lens-based scanning, RESOLFT [15]) or, albeit more rarely, to more precisely control fluorescence events in single-molecule imaging super-resolution techniques [16] (for example PALMIRA [17]). Additionally, the unique kinetic footprints of the different switching proteins can be used to allow temporal unmixing of cell populations [14] even in whole transparent organisms [18].
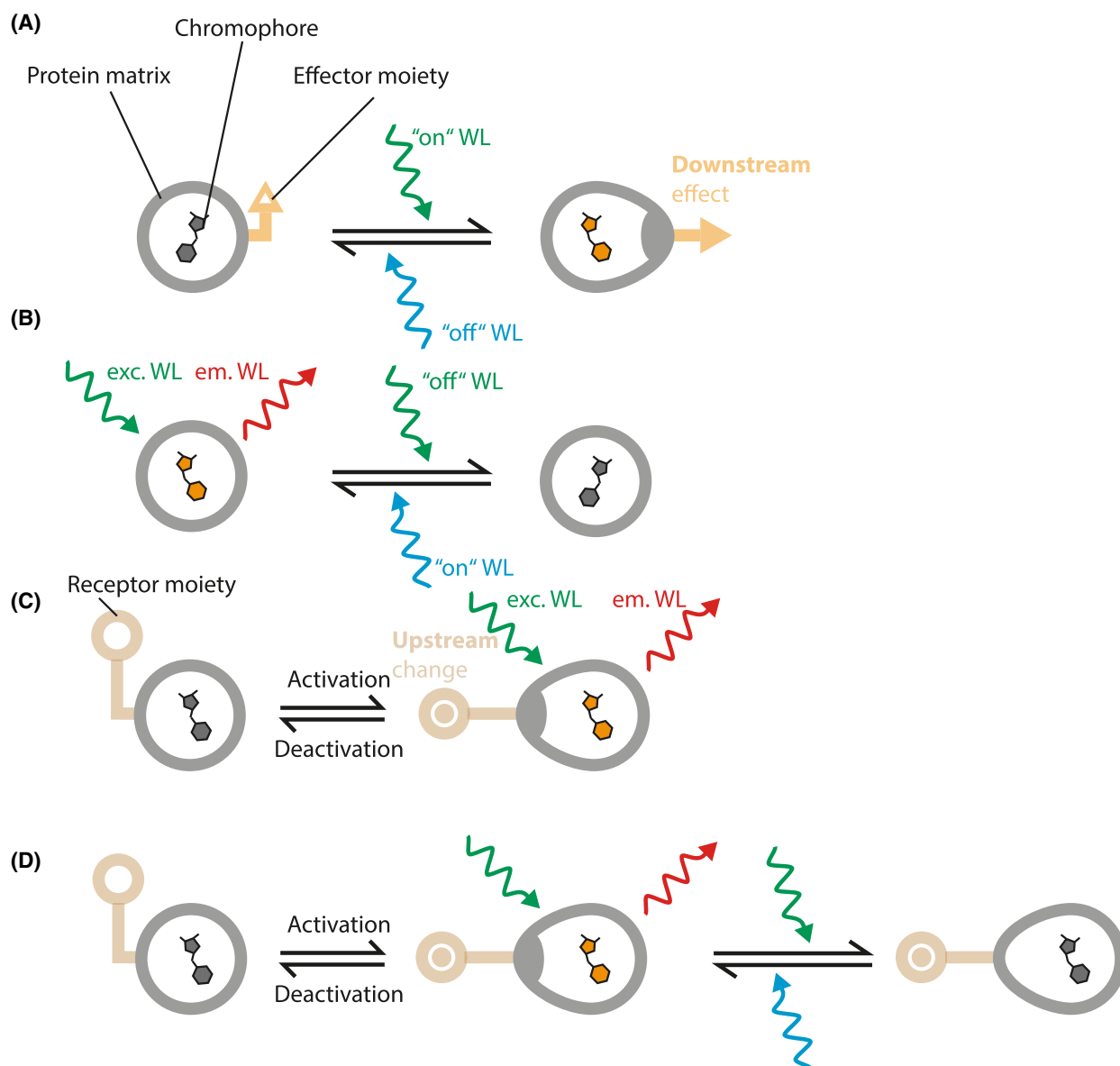
Fig. 1. Different scenarios of interaction between the protein matrix and chromophore. (A) Light induces chromophore isomerization (gray to yellow change of chromophore), resulting in alteration of the protein matrix (bulging of circle) and a subsequent downstream effect (effector moiety). Colors denoting illumination are chosen for maximal distinguishability and do not represent actual illumination WL. (B) Light induces isomerization leading to a change in photophysical properties, e.g., switching between fluorescent and nonfluorescent forms. (C) The protein matrix is affected by an upstream change (receptor moiety) leading to altered photophysical properties. (D) Upstream change alters protein matrix and thus chromophore photophysics leading to, for example, the possibility to photoswitch.

In contrast to native BphPs, RSFPs do not seem to have a downstream biological function for their photoswitching—indeed, the β-barrel fold of FPs leaves few vantage points for downstream effects. Nonetheless, the protein matrix around the chromophore is highly crucial for shaping RSFP's photoswitching behavior. In fact, photoswitching is only one aspect of the photophysical versatility enabled by the β-barrel fold and the chromophore of FPs (see FPbase.org for a comprehensive impression [19]). The majority of RSFPs to date are green and the development of red RSFPs is challenged by complex photophysics, low fluorescence quantum yields, and photofatigue (see Table S1 for basic figures on the proteins mentioned in this review). Taking the example of rsCherry/Rev [20], its use in RESOLFT is
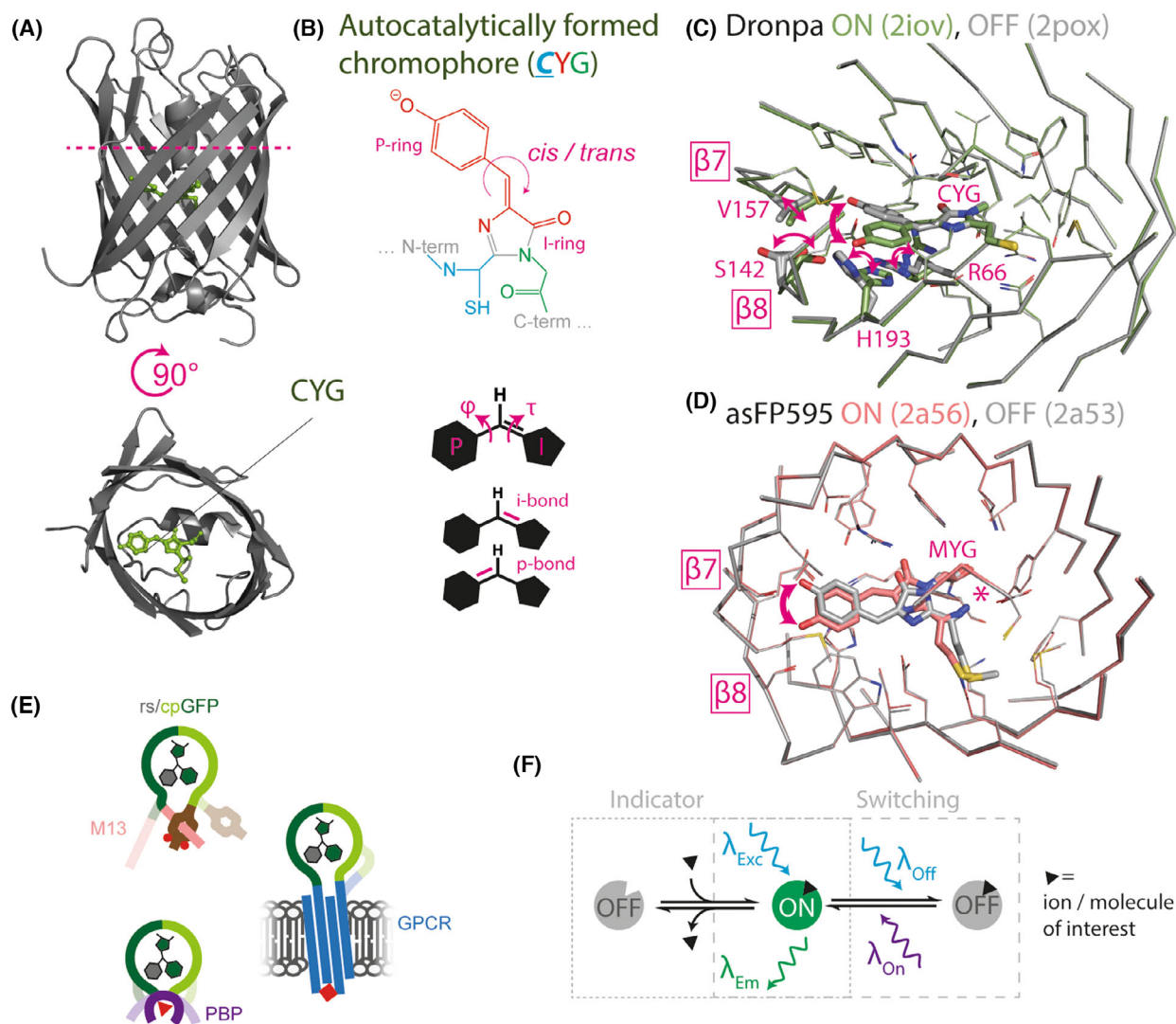
Fig. 2. Photoswitching proteins of the GFP-like family (RSFPs). (A) Representative structural overview (here Dronpa, 2iov) showing the 11-stranded β-barrel enclosing the central α-helix with the chromophore. In the 90° turned representation, the top part of the protein (dashed line) is omitted for clarity. (B) Top: Representative chromophore (here Dronpa) showing the p-hydroxyphenyl (P-ring) and imidazolinone (I-ring) and the methine bridge involved in *cis/trans* isomerization. The bonds and atoms are colored according to the amino acids contributing to the autocatalytic chromophore formation. While tyrosine and especially glycine are largely conserved, the first amino acid (here **c**ysteine) is highly variable. Bottom: bonds of the methine bridge that can contribute to the *cis/trans* isomerization. (C) ON- and OFF-state structure of Dronpa. The residues that undergo conformational rearrangements (arrows) are denoted along with the β-strands that show flexibility. (D) ON- and OFF-state structure of asFP595, a protein that shows almost no change of the protein matrix upon photoswitching; the same β-strands as in c are marked for orientation. The main chain break, characteristic of asFP595, is indicated by an asterisk. (E) Different concepts of building (photoswitching) chimeric sensor proteins. Clockwise: calcium sensor based on Calmodulin with an M13 or RS20 peptide, GPCR-based sensor, and PBP-based sensor. (F) Concept of photoswitching small molecule sensors.

limited by long-lived states not contributing to fluorescence emission, oligomerization tendencies and possibly the photodestruction by oxygen [21]. The recently developed class of rsFusionReds somewhat overcomes those challenges [22] but is still inferior to most green RSFPs.

Many molecular mechanisms of RSFPs have been clarified by x-ray crystallography of equilibrium and photoswitched states (Table S2). Due to the rigidity of the β-barrel, it is readily possible to photoswitch proteins in the crystallized form [23]. Such datasets allow a highly congruent comparison between states, in

order to explore the interplay between protein matrix and chromophore. Based on insights from end-state structures (ON- and OFF-state), the structurally apparent effects can be grouped into three categories: (a) how the chromophore isomerizes, (b) to what extent photoswitching alters the conformations of chromophore-surrounding residues and lastly (c) to what extent the backbone of the β-barrel is displaced (Table S2). Beyond that, in recent years, time-resolved structural and spectroscopical methods have painted a clearer picture of the dynamics of the photoswitching process.

Photoswitching mechanisms in RSFPs

Key to all photoswitching in proteins is the absorption of a photon by a chromophore resulting in a photochemical conformation change of the chromophore. For RSFPs, this change is most commonly linked to a *cis*/*trans* isomerization over the methine bridge connecting the p-hydroxyphenyl and imidazolinone rings of the chromophore (Fig. 2B). The *cis* isomer is commonly the fluorescent ON-state similar to nonswitching FPs, except in some cases such as eqFP611 [24] where *trans* is the fluorescent ON-state. The photoswitching results in changes of the chromophore with respect to the protein matrix. Structurally, the *cis*/*trans* isomerization of the chromophore can occur as a flip over the τ bond of the methine bridge (one bond flip, OBF), resulting in a major displacement of the p-hydroxyphenyl ring. Alternatively, an isomerization involving movements about both the φ and τ bond can occur. This isomerization, vividly termed hula twist (HT) (Fig. 2B), is much more space-conserving. HTs are not limited to RSFPs but are also found in photo-active yellow proteins [25] or BphPs (see below). Moreover, HTs occur in numerous dyes [26], with the solvent influencing the isomerization pathways [27].

This change of chromophore conformation and the immediate chromophore environment is often accompanied by protonation/deprotonation events of the chromophore leading to photochromism, where the neutral chromophore is more blue-shifted and the anionic more red-shifted. This influence on the spectral characteristics allows for the use of distinct and discrete WL for photoswitching (for a mechanistic overview, see Duan *et al*. [28]). The photoswitching-dependent protonation states of the chromophore are related to similar protonation states in nonswitching FPs, which can be accessed through pH titrations. The dependencies between light-induced and pH-titration-induced protonation states and chromophore isomerization are not uniform among FPs. For example, the

red protein mKate [29] shows an isomerization that can be induced through pH changes. The structure of mKate at acidic pH (pH 2) shows a protonated chromophore in *trans* conformation, while at neutral pH (pH 7), it is deprotonated and in the *cis* conformation. Additionally, the remaining population of the *trans* state can be photoswitched [29]. It is speculated that the change in pH leads to variations in the electrostatic field of the chromophore surrounding, affecting the state-stabilizing hydrogen bonds, which could potentially trigger the isomerization [29]. A recent study of the RSFP rsFolder also revealed chromophore isomerization states interchangeable by pH in the dark [30]. Interestingly, here the population does not fully isomerize but the *trans* isomer population shows a peak at pH 5 (30%) before decreasing again at lower pH. This behavior is likely linked to the protonation states of H149 (148, for all residues in this section, GFP consensus numbering is given in brackets). By contrast, Dronpa exhibits an acid-induced protonated chromophore that does not seem interconvertible with the photoswitching-derived chromophore [31].

Beyond *cis*/*trans* isomerization, other mechanisms can drive photoswitching. For example, Dreiklang, a photoswitching protein engineered from Citrine, shows photoswitching *via* reversible hydration of the chromophore [32]. Dreiklang is also one of the few RSFPs that shows photoswitching with two WL (365 nm and 405 nm) while fluorescence can be excited by a third (515 nm). The chromophore in the ON-state shows absorption at 405 and 515 nm. When illuminated at 405 nm, a hydration reaction that adds a hydroxy group from an ordered water molecule to the imidazolinone ring occurs. This shortens the π-electron system and disrupts the planarity of the imidazolinone ring of the chromophore giving rise to the OFF-state. The OFF-state can be converted back to the ON-state with illumination at 365 nm, which causes dehydration. Recently a natural FP with such a three-WL switching property has been identified from *Aequorea australis* [33].

Photoswitching, in particular *via* *cis*/*trans* isomerization, is already manifested in the chromophore itself, as exemplified by studies on purified chromophore analogs [34] and computational studies [35]. This indicates that the potential for photoswitching is inherent to the class of GFP-like FPs. For instance, even GFP with a single mutation (E222Q) displays rudimentary switching [36]. Despite this relationship between non- and photoswitching FPs, few natural photoswitching FPs exist (e.g., asFP595, 22G, or eqFP611) and the majority of RSFPs are engineered. The small number

of natural RSFPs might be attributed to their lack of known native functionality and that photoswitching, next to the intrinsic chromophore properties, relies on the precise shaping of the protein matrix which allows for accessibility and stability of a switched state.

Interplay between the chromophore and surrounding residues in RSFPs

The protein matrix surrounding the chromophore shapes the electrostatic environment, stabilizes or restricts chromophore conformations by steric effects, and provides partners for noncovalent interactions (hydrogen bonding, salt bridge, or van der Waals). This environment shapes the transitions between the photoswitched states and governs their stability and photophysical characteristics. The light-induced excited state transitions are considered to be defined primarily by electrostatic [37] interactions while thermal ground state transitions are primarily influenced by sterical effects. The pKa of the chromophore is influenced *via* the immediate electrostatic surrounding and the stabilization of distinct chromophore conformations (i.e., torsions of the methine bridge bonds [38]). Furthermore, the conformational stabilization of the chromophore is instrumental for the presence or absence of fluorescence by reducing conformational dynamics (nonradiative de-excitation) and increasing planarity. In fact, it shows that the absolute value of the sum of the methine bridge torsion angles φ and τ is always smaller for the fluorescent state than the nonfluorescent state [39]. Hydrogen bonding networks have a debated effect on the photoswitching quantum yield (likelihood of photoswitch). A recent study on rsGreen suggests a linkage between an increased number of hydrogen bonds with water molecules and high photoswitching quantum yield, due to a larger number of chromophore forms that can be stabilized by the dynamic water network, including those accessing the *cis/trans* isomerization [40]. By contrast, an *in silico* study on Dronpa-M159T suggested that a larger number of hydrogen bonds prevented photoswitching [41]. However, the *in silico* work also emphasizes the strong fluctuations of (water to chromophore) hydrogen bonds that allow the sampling of conformations with fewer bonds leading to photoswitching. Hence, the two studies converge in assessing the importance of conformational sampling in the ground state for access to the *cis/trans* isomerization. The influence of the protein matrix on a protein's photoswitching kinetics and eventual suitability for imaging applications is best exemplified by the numerous engineered variants with properties more favorable for applications,

predominantly in super-resolution imaging [42]. For example, the massive influence exerted by just a single position is illustrated by the variant Dronpa-M159T [43] (167, also known as Dronpa 2 [44]), which shows a 1000× accelerated photoswitching and thermal relaxation of the switched state compared with its parent Dronpa [45]. The exact interdependencies, intermediates, and succession of events in photoswitching are very diverse and researched for a number of RSFPs with excellent reviews summarizing the insights [28,46–49].

Rearrangements of surrounding residues

The interplay between chromophore isomerization and the rearrangement of the surrounding residues is of particular interest from the perspective of this review. While end-state structures suggest a link between certain chromophore displacements and residue rearrangements (Table S2), it can be challenging to determine the details of the actual transitions. For example, RSFP rsEGFP2 exhibits stable end states of the *cis* and *trans* chromophore with a large displacement of the chromophore, intuitively suggesting an OBF. However, infrared spectroscopy measurements [50] and serial femtosecond crystallography (SFX) structural assessments [51,52] suggest instead an HT, with the chromophore develop into the more space-consuming end position through rearrangements for *trans* → *cis* [50] (Fig. S1) and for *cis* → *trans* [51,52].

Nonetheless, there are notable examples of both, strong rearrangements of chromophore-surrounding residues or, opposingly, of no rearrangement despite chromophore isomerization. The most prominent example of strong rearrangements of the protein matrix in photoswitching can be found in the RSFP Dronpa [45] (Table S2). Endpoint x-ray structures show that the isomerization of the chromophore is accompanied by changed conformations for R66 (69) and H193 (203). Additionally, S142 (148) and V157 (165) rearrange away from the chromophore, resulting in a slight displacement of β-strand 7 and 8 by ~ 0.6 Å each [53] (Fig. 2C). Similar rearrangements have been found for Skylan-NS [54]. RsEGFP2 shows a significant outward displacement of β-strands 7 and 8 but fewer conformer changes of the chromophore-surrounding residues Y146 (145) and H149 (148) [55].

On the other hand, some proteins do not exhibit any changes in the protein matrix upon photoswitching. In certain cases, this can be explained by peculiarities of the chromophore, such as a break of the backbone, as in asFP595, potentially linked to the space-conserving HT, as indicated from molecular

dynamics simulations [56–58] (Fig. 2D). Remarkably, Padron, a derivate of Dronpa, shows a similar space-consuming displacement of the p-hydroxyphenyl as described for its parent above but without similar residue rearrangements [59]. Notably, crystals of Padron can also be photoswitched at cryotemperatures (100 K) [59], demonstrating the negligible involvement of protein matrix rearrangements. The nonfluorescence of the Padron *trans* state, despite its deprotonated chromophore, is primarily attributed to a strong torsion of the chromophore in this state [39]. This torsion is likely linked to limited rearrangements as it is forced by a fixed conformation of R66 (69), which in turn is stabilized by a cascade of effects stemming from the Padron mutation P141L (147). R66 is often found forming a salt bridge with E144 (150) in β-strand 8 which anchors to a certain extent the β-strand to the central α-helix. In parent Dronpa the rearrangement of R66 in photoswitching likely alters this stabilization permitting β-strand displacement.

Influences of photoswitching on the β-barrel

NMR studies with (His)-$^{13}C_{6,15}N_3$- [60] and complete backbone-labeling [61] have shown that the extensive rearrangements observed in Dronpa are linked with a pronounced flexibility of the β-barrel, especially the β-strands on the p-hydroxyphenyl side of the chromophore - a phenomenon termed a 'dynamic polymorphic state' [60] or β-barrel 'breathing'. This phenomenon is not only associated to photoswitching, but similar backbone dynamics, in particular of β7, β8, and β10, have been observed in GFP. This suggests that β-sheet flexibility of these strands is a general possibility in FPs [62]. Studies of Dronpa have confirmed the influence of β-barrel mobility on photoswitching, as photoswitching slows down with increased viscosity due to the restricted barrel dynamics [63]. In agreement, β-barrel mutations with reduced sidechain size like Dronpa-M159T (β-strand 7) may accelerate switching due to less hindrance to chromophore isomerization; however, it must be considered that the mutation might lead to a change in the hydrogen bond network.

SFX can capture dynamic processes and has provided valuable insights into the transient aspects of structural interplay; moreover, these methods have allowed for observations at room temperature (RT) [23]. For rsEGFP2, several studies show transient states after photoexcitation along with findings on the general flexibility of residues in β-strand 7 [52], pointing to a similar β-barrel 'breathing'. The temporal

development of the photoswitching interplay between the chromophore and surrounding protein matrix is exemplified by structures of rsEGFP2 at 10 ns after ON-switching laser illumination (400 nm). The data reveal that the chromophore already isomerized to *cis* state while only partial residue rearrangements have occurred: Y146 (145) is already in its later ON-state position, but H149 (148) remains in an OFF-state conformation [51]. Additionally, the studies revealed are markable finding: the existence of a second *trans* conformation besides the space-consuming *trans* conformation typically observed in synchrotron structures [51]. This second conformation is visible at RT and has occupancies of roughly ¼ of the total off-state *trans* chromophore population. It is more similar to space-conserving *trans* conformations that can be accessed *via* HT. Possibly, this hints at additional rearrangement processes of the chromophore in addition to the isomerization itself (see above) [50]. It is fascinating to note that mutations at position V151 (GFP = 150 in β-strand 7 result in different occupancies for the two *trans* states at RT [64]. This suggests a coexistence of both *trans* conformations, with subtle details of the protein matrix governing the populations —termed 'switching fragility' in the article [64]. Lastly, rsEGFP2 studies using a chlorinated chromophore could distinguish the bond rotational contributions of OBF and HT and provide further evidence for the interplay between overall protein matrix flexibility and chromophore isomerization [65]. The research revealed that the packing of the matrix—here artificially limited by a restricted unit cell—determines the isomerization pathway, with HT being favored in more restricted conditions. Additionally, it is worth noting that rsFolder [55], a GFP-based RSFP related to rsEGFP2, shows a second more space-conserving *trans* conformation similar to the one observed in rsEGFP2 [55,64]. NMR studies revealed strong structural dynamics in residues of the β7 and β8 strands upon illumination [66], demonstrating the structural flexibility of those regions during switching, thus possibly accommodating the transition without too many side chain rearrangements, as it is observed in the end-state structure [55].

The impact of chromphore rearrangements on the β-barrel structure also becomes more intuitive when considering the reciprocal effect where pressure on the β-barrel influences chromophore photophysics. This effect was shown for several FP variants [67–70] that exhibit spectral shifts upon pressure changes. Likely, the pressure on the β-barrel scaffold leads to subtle residue rearrangements, which influence the

hydrogen bond network or the chromophore planarity directly [69,70].

Exploitation of β-barrel dynamics to create optogenetic-like approaches

The structure of the β-barrel fold does not leave room for long-range structural effects; nonetheless, the small displacements that can occur upon photoswitching of RSFPs have been exploited to convey effector functions that allow for control over protein activity (optogenetics). For instance, in the case of Dronpa, the transient β-strand displacement that occurs upon chromophore isomerization has been utilized to create a light-switchable structural element that enables reversible monomerization and re-oligomerization. The first evidence linking oligomerization with photoswitching came from a study investigating a mutation in β-strand 7, which is part of the cross-dimer interface in the tetrameric Dronpa parent 22G [45]. The K145N mutation, located in the dynamic polymorphic state' area as identified by the NMR measurements mentioned above, leads to oligomerization at high concentrations, as it presumably strengthens the dimer interface between chain A and C, while the variant is monomeric at low concentrations [71]. Importantly, the tetramer present at higher concentrations can be dissociated by cyan illumination (500 nm) and reconstituted by violet illumination (400 nm) [72], suggesting that the position of the *trans* chromophore relative to β-strand 7 disrupts the dimer interface, in the K145N variant. Potential uses were demonstrated for light-activated HCV proteases [72], Cdc42 activation [72], and kinases [73]. Of note, the monomer present at lower concentrations of the K145N variant exhibits an accelerated photoswitching [74]. Conversely, the tetramer likely hinders the barrel bulging, thereby hampering the matrix reorganization during photoswitching and leading to slower switching. This is corroborated by the slower switching of the tetrameric parent of Dronpa 22G relative to the Dronpa monomer [74], and is in line with the viscosity dependence mentioned above.

Photoconversion in combination with photoswitching

Besides photoswitching, FPs show other photoresponsive behaviors like photoactivation (illumination permanently converts protein into a fluorescent state) and photoconversion (illumination permanently converts protein from a green absorbing to a red-absorbing state). Several photoconverting proteins show additional photoswitching behavior, such as pcDronpa [75]

and IrisFP [76], which are members of the Dronpa and mEos clade, respectively. These two proteins show photoswitching behavior in the green state and can also be photoconverted to a red state by UV light (405 nm), following the same mecanism as in nonphotoswitchable convertible FPs. This process is governed by a breakage of the polypeptide chain upstream of the first chromophore amino acid, which in the case of green-to-red conversions, is exclusively a histidine. The cleavage leads to a reorganization that effectively extends the π-electron system to include the his tidine imidazole sidechain, leading to the red shift. The structures of the green ON-state and the photoconverted red state show no further change. However, unlike pcDronpa, IrisFP can photoswitch also in the red state. The differences in chromophore packing between IrisFP and pcDronpa are key to their photoswitching ability. In the red-state, the *cis*-chromophore in pcDronpa is more fixed than in IrisFP, suggesting a higher QY for the fluorescence decay and a decrease in the nonradiative channels including isomerization [75]. Crystallographic data suggest a space-consuming isomerized position, likely accessed through an OBF, for the red state isomerization as well [75]. Beyond that, IrisFP exhibits faster thermal ground state relaxation for the red photoswitching possibly due to the increased chromophore flexibility resulting from the broken backbone. Recent research on mEos4b, a photoconverting member of the mEos clade thought to be nonphotoswitching, further suggests that all FPs have varying degrees of 'predisposition' for photoswitching and other photoresponsive behaviors. The authors elucidated a long-lived dark state for the red-converted form of mEos4b, which can be swiftly recovered with blue illumination, hence suggesting a photoswitching behavior [77]. The fact that the parent clades of both, IrisFP and pcDronpa have members capable of only photoswitching, only photoconversion or both switching and conversion, as summarized recently for mEos [78], exemplifies the mentioned 'predisposition' for the different photoswitching behaviors that can sometimes be 'manifested' by only a few mutations.

It is worth noting that the backbone break introduced by photoconversion has been harnessed to develop optogenetic tools showing light-induced irreversible dissociation. The green-to-red convertible protein mMaple was topologically changed (canonical β-sheet numbering: N-β4–β11-linker-β1–β3-helix-C), leaving the central α-helix with the chromophore at the C-terminus. After photoconversion and consequent backbone breakage, this allows for the dissociation of a 10-residue small C-terminal fragment containing the chromophore, leaving behind an empty β-barrel [79]. This approach has

been used to achieve light-activatable unblocking of a protease [79], among other applications.

Single-FP sensors—upstream structural influence on photophysics

The interplay of light-induced chromophore alteration and protein matrix has only recently been linked to another field of protein matrix-mediated chromophore influence namely FP-based biosensors. Such sensors allow for the noninvasely reporting of small molecule and ion distributions from inside a cell or organism, by linking the binding of the molecule of interest to a receptor with a measurable signal change, such as fluorescence. For an excellent, extensive, and detailed review on the multitude of possible designs, see Greenwald *et al.* [80]. The class of single-FP sensors is particularly interesting when considering the interplay between protein matrix and chromophore, since the receptor moiety and FP are directly coupled (chimeric sensors). Upon binding of the target small molecule or ion, an upstream structural change of the receptor moiety directly alters the chromophore environment of the FP, leading to a readout (Fig. 1C). This functionality was enabled by the introduction of the circularly permuted GFP [81]. Here, the N- and C-termini of GFP are closed at the bottom of the barrel with a linker, and new N- and C-termini are opened in β-strand 7 in the center of the barrel, at the level of the chromophore, allowing a direct structural relay mechanism. Many sensors have been built using this strategy (Fig. 2E), including well-known calcium sensors [82] based on calmodulin and M13/RS20 peptide (e.g., GCaMPs), as well as sensors using the class of periplasmic binding proteins (PBPs) or GPCRs [83]. All these sensors affect the chromophore's protonation without changing its isomerization state (known up to now).

Combining sensing and light-induced chromophore alterations

Recently, a number of publications have combined single-FP sensor concepts with light-induced chromophore changes. This means that protein matrix changes induced by the binding of the molecule of interest exert control over the photoswitching or conversion propensity of the chromophore. In the CaMPARI sensors [84,85], coupling of a circularly permuted version of the photoconvertible protein mEos to Calmodulin and M13 yielded a sensor that is effectively photoconvertible with UV light from the green to the red state only in the presence of calcium. Thus, the green form can be used to visualize calcium concentrations like

conventional green calcium sensors, while the red-converted form allows the permanent marking of calcium-rich regions, providing a 'snapshot' that can be used, for example, in circuitry mapping. The exact mechanisms for FP photoconversions are still under debate, but in general they are likely to involve proton transfers, structural twisting of the chromophore, and potential radical formation caused by UV irradiation [78]. It is evident that such mechanisms are only possible with a well-defined chromophore environment; for CaMPARI this is only achievable if calcium-binding 'closes' the β-barrel *via* Calmodulin and M13, allowing a coordinated environment for the chromophore. The same authors subsequently introduced a photoswitchable CaMPARI (rsCaMPARI) [86], which can be effectively switched to a state with dim fluorescence (so-called 'negative switching') only in the presence of calcium [86]. Thus, the reversibility allows repeated cycles of marking and erasing of the same sample, for example, to map the calcium response of neurons to different stimuli in one experiment.

Since photoswitching confers significant advantages to super-resolution or photo-modulation-based imaging techniques, it would be beneficial if those advantages could also be applied to sensor imaging. However, the rsCaMPARI is unsuitable for such approaches since the low calcium form retains a considerable level of fluorescence. By contrast, RSFPs routinely used in super-resolution imaging should ideally switch to a complete OFF-state. Here, the introduction of photoswitchable GCaMPs introduced new possibilities (Figs 1D and 2F) [87]. By exploring the mutational space around the chromophore and including known mutations conveying photoswitching in rsEGFPs, GCaMP5G was rendered photoswitchable. This means that reversible photoswitching between an ON- and OFF-state with 488 nm and 405 nm light is only possible in the presence of calcium. Lack of calcium leaves the sensor nonfluorescent and nonswitchable (Fig. 2F). The conceptual use in imaging was demonstrated both by targeting rsGCaMP to the endoplasmic reticulum and by implanting the sensor subcutaneously in mice, demonstrating super-resolution and optoacoustic imaging, respectively (for an explanation of the method, see the BphP section). However, current versions of the sensor are limited by a low brightness in the calcium-bound switched ON-state, which complicates imaging [87]. Interestingly, structural data of rsGCaMP in the calcium-bound form in its fluorescence ON- and nonfluorescent OFF-state revealed a chromophore showing exclusively a space-conserving position in contrast to the space-consuming end position available in the parent

rsEGFP2. The tight packing of the calcium-bound calmodulin/M13 complex to the flank of the β-barrel likely restricts its movement, thus enforcing an HT of the chromophore or at least preventing the rearrangement from the HT to the space-consuming positioning seen in rsEGFP2, as discussed above. Along these lines, the *trans* state in rsGCaMPs is likely similar to the alternative *trans* state mentioned above, which was revealed *via* time-resolved crystallography and in the constricted unit cell of rsEGFP2. Moreover, in the structure of calcium-bound rsGCaMP, position 151 (which, when mutated in rsEGFP2 caused a shift in the population of the alternative *trans* states [64]), is situated far more inward (~ 1 Å) than in rsEGFP2. The inward shift of position 151 in rsGCaMP (due to the packing of calmodulin/M13) likely biases the *trans* state population towards the alternative space-conserving *trans* conformation.

Concomitantly, a similar type of sensor, GCaMP6s-Q [88] was introduced. The group used the calcium-dependent photoswitching abilities of this sensor class for the absolute quantification of calcium from signal readouts. In a method termed photochromism-enabled absolute quantification (PEAQ), the authors use the calcium-dependent photoswitching contrast, i.e., $\Delta F/F_0$ upon illumination, obtained in a calibration measurement with exact calcium concentrations to extract absolute concentrations from measurements in cells [88]. The photoswitching kinetics of the sensors from both groups show a dependence on the calcium concentration, however the reason for this phenomenon is under debate. One possibility, proposed for rsGCaMP, would be that at lower calcium concentrations, the sensor population is a mix of sensors with two or four bound calcium ions, the former is known to exist for Calmodulin and theorized for GCaMPs [89,90]. Differently occupied sensors can have different structures and hence photoswitching characteristics [87]. Another proposed mechanism, albeit with the slightly different GCaMP6s-Q, explains the phenomenon with only one species of calcium-bound sensor, but with inverse switching in the calcium-bound and free state (negative and positive, respectively), as well as photoswitching-dependent calcium-ejection (at very low analyte concentrations) [91]. The latter would interestingly close the loop to RSFPs like the Dronpa variant K145N, for which photoswitching exerts a downstream effect *via* the protein matrix. Furthermore, it has been shown that the concept of photoswitching sensors not only applies to GCaMP but also extends to sensors relying on periplasmic binding proteins (PBP) or GPCRs as receptor moieties [87]. The photoswitching PBP- and GPCR-based sensors were built with receptor moieties already used for nonswitching FP-based sensors [83,92], suggesting that in general chimeric sensors can be rendered photoswitching.

Bacteriophytochromes

Photoswitching mechanisms of BphPs

Phytochromes are a superfamily of chromophore-bearing proteins found in plants, fungi, and bacteria, that play important roles in numerous light-regulated processes including germination, phototropism and phototaxis [95]. Phytochromes are established photosensory scaffolds for optogenetics [96] and have also gained attention for their potential advantages in optical imaging due to their far-red absorbance, stemming from a prosthetic open tetrapyrrole chromophore. This absorbance range makes them ideal for cell and tissue imaging due to reduced photo-damage and lower scattering at far-red wavelengths, while also expanding the spectral range available for multiplexed imaging [97]. A defining feature of native phytochromes is that they exist in two stable states with different spectral characteristics: a red light-absorbing state (P_r, max ~ 700 nm) and a far-red light-absorbing state (P_{fr}, max ~ 750 nm). These two states can be reversibly photoswitched by far-red and red illumination, leading to downstream effects on biochemical activity, and a range of cellular responses [98–100].

Phytochromes can present a variety of bilin chromophores; however, most of them, like phycoerythrobilin or phycocyanobilin, are only readily accessible in non-mammalian organisms (e.g., red algae and cyanobacteria). In contrast, BphPs are highly useful for mammalian cell or tissue imaging because their chromophore is biliverdin IXα (BV), a product of heme catabolism and thus ubiquitously present in most mammalian cell types [101]. The canonical structure of BphPs consists of three domains in the order PAS, GAF, and PHY (phytochrome-specific), which together form the protein photosensory core module (PCM, Fig. 3A). C-terminally, those domains are followed by a variety of effector domains forming the output module (OPM). In general, the high diversity of effector domains and OPM configurations in BphPs, and even more so in phytochromes, allows for a range of biological functions and regulatory mechanisms. Native BphPs act in bacterial intracellular signal transduction, namely in phosphorylation and dephosphorylation reactions and second messenger metabolism [100].

The BV chromophore is covalently-bound to a cysteine residue in the PAS domain, but it is primarily enclosed in an extensive noncovalent interaction

network within a cavity in the GAF domain [102,103]. The PAS-GAF domains are thus sufficient to bind BV and form the chromophore-binding domain (CBD). Furthermore, the chromophore pocket is closed by a protruding loop from the PHY domain (~ 30 residues) referred to as the 'PHY tongue', which is crucial for photoswitching and consequent conformational signal relay. Two long α-helices connect the GAF and PHY domains and the PHY and OPM domains, respectively. Together, within the BphP structure, they form the 'helical spine' that is responsible for the light-activated conformational relay along the protein, eventually activating the OPM and downstream cellular responses. BphPs natively form dimers, canonically head-to-head, via interfaces in the PAS-GAF domain and the spine helix-OPM region. The BphPs' quaternary structure plays a central role in the light-driven activation of the OPM.

Overall, the distinctive architecture of BphPs and phytochromes in general, is key to their functional hallmark: a fascinating transduction from light absorption to a widespread structural rearrangement of the protein matrix, ultimately leading to downstream effector functions. The light-activated signal relay within the structure of the BphPs can be divided in three aspects: (a) the light-induced chromophore isomerization and consequent rearrangements in the chromophore's immediate protein surrounding, (b) the local changes that trigger structural shifts in the overall PCM, and finally, (c) the OPM regulation by this switch, culminating in biological activity.

The chromophore pocket: light-driven state transition and changes in the immediate chromophore environment

Bacteriophytochromes are capable of converting absorbed light energy into conformational changes in the protein. The heart of this process is a light-induced isomerization of the BV tetrapyrrole chromophore over the methine bridge connecting pyrrole ring C and D, from a *cis (ZZZssa)* to *trans (ZZEssa)* configuration (Fig. 3B). This isomerization effectively changes the orientation of the D-ring relative to the protein matrix (Fig. 3C). The canonical equilibrium state is the red-absorbing P_r state with the chromophore in its *cis* conformation; exceptions are the so-called bathy phytochromes, which thermally relax predominantly into the *trans* chromophore P_{fr} state [104,105]. The reversible light-induced photoswitching between the two stable states P_r and P_{fr} progresses over a series of short-lived intermediates (canonical: $\mathbf{P_r}$ → Lumi-R → Meta-Ra → Meta-Rc → $\mathbf{P_{fr}}$; $\mathbf{P_{fr}}$ → Lumi-F → Meta-F → $\mathbf{P_r}$, Fig. 3B). The exact dynamics and photophysical details largely differ among BphPs and are still under investigation for most species [106]. However, some common elements have been clarified mainly by spectroscopic data and, more recently, in a structural study of cryo-trapped intermediates for the back conversion from P_{fr} to P_r [107]. The photoexcited P_r state relaxes in tens of picoseconds with the occurrence of the BV *cis/trans* isomerization about the methine bridge, forming the Lumi-R intermediate [108–112]. Possibly due to the spatial constraints of the chromophore pocket, the D-ring methine bridge rotation follows an unconventional HT mechanism [113,114], similar to that observed for some RSFPs. The P_r-to-P_{fr} transition has a low quantum yield of 15%, competing with the decay back to the ground state of P_r; interestingly, this quantum yield is quite consistent throughout native BphPs [108–110]. As in RSFPs, the switching quantum yield is determined by the hydrogen bonding network around the D-ring, since the rupture of state-stabilizing bonds poses the rate-limiting step [108,115]. From Lumi-R, the chromophore undergoes sequential deprotonation and protonation

Fig. 3. Natively photoswitching BphPs. (A) Overview of the multidomain architecture of BphPs on the example of IsPadC (5llw). GAF domain is rainbow-colored from N to C. The chromophore (BV) and 'PHY tongue' are highlighted separately. The 'helical spine' α-helices are additionally augmented by magenta lines along with the domain of the respective part of the 'helical spine'. (B) Biliverdin (BV) chromophore has four pyrrole rings; the methine bridge between rings C and D is involved in the *cis/trans* isomerization. (C) Chromophore pocket in the *cis* and *trans* state. Color-coded as in a, only residues with major involvement in the photoswitching are shown as sticks together with their respective polar interactions. Outtake corresponds to the dotted square in 'A'. (D) Twisting of the 'helical spine' and OPM domain upon photoswitching (here 5llw and 6et7 an IsPadC variant that stabilize the switched form). The *cis* and *trans* structures in surface representation are colored according to the dimer interface contacts they make: green = contacts in *cis* and *trans*, red = contacts only in *cis*, and green = contacts only in *trans*. The interface in the OPM subjected to the primary change is indicated with arrows. (E) Schematic representation of a noncircular-permuted chimeric calcium sensor based on BphP. (F) Topological representation of a BphP (here IsPadC). 1 = helix that is regularly used to elongate into chimeric OPMs to construct optogenetic tools from BphPs; 2 = truncation sides for Per-Arnt-Sim (PAS)-GAF only fluorescent BphPs; 3 = entry sides identified for a circular permuted PAS-GAF BphP leaving a folded protein; 4 = entry side for PAS-GAF based sensor engineering identified by Qian *et al.* [93]; 5 = entry side for sensor engineering identified by Subach *et al.* [94].
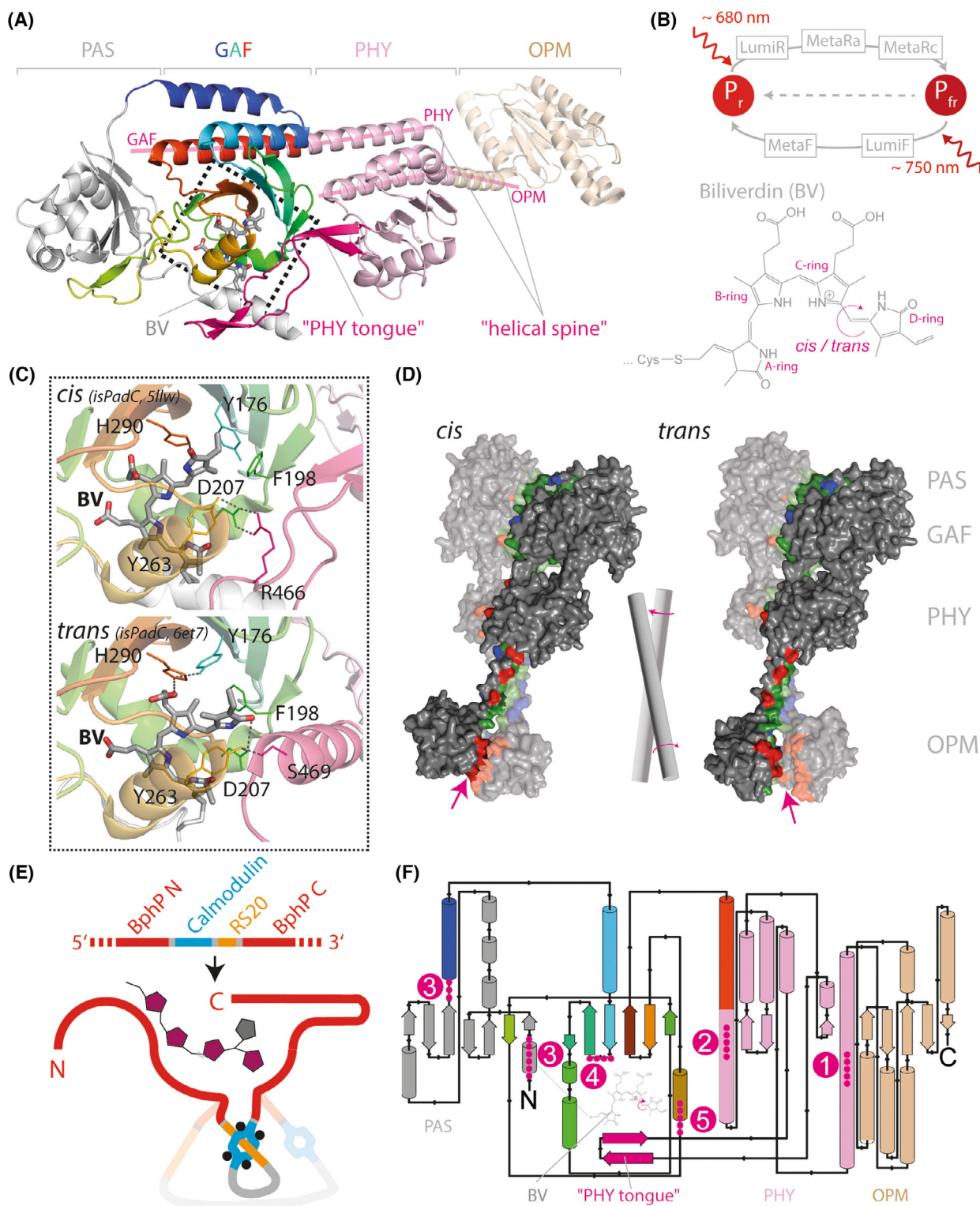
events that last tens of microseconds and result in the Meta-Ra and Meta-Rc intermediates, respectively [116,117]. At last, the Meta-Rc intermediate transitions into the final stable P_{fr} state on a millisecond scale [116]. For the transition back from P_{fr} to P_r, evidence shows the chromophore stays fully protonated, and

the transition and corresponding BV isomerization occur in two steps, which are somewhat faster than those for the P_r-to-P_{fr} transition [118,119]. The excited P_{fr} quickly decays (1 ps) to Lumi-F [108–110,120], which in turn decays in microseconds to the Meta-F intermediate, where the hydrogen bond network between BV and the pocket is rearranged, with the final transition to P_r occurring within milliseconds [118,121]. It should be noted that unlike RSFPs, the P_r and P_{fr} end states of BphPs commonly show the BV chromophore with the same protonation, indicating that the spectral signature of the photochromism is solely governed by the steric arrangement of the BV molecule and its surroundings. Apart from the light-induced excited state transitions, BphPs can revert to their equilibrium state *via* thermally-driven dark state relaxation. The relaxation times are highly dependent on environmental factors such as pH, ionic strength, reducing agents, metal concentrations, and temperature [106,122]. Interestingly, some BphPs also show pH- [123] or temperature- [124,125] dependent photoconversion and activity. This opens the possibility that the interplay between dark state relaxation and photoswitching in BphPs.

Structural rearrangements in the vicinity of the chromophore

The structures of BphPs in both the P_r and P_{fr} stable states have provided detailed insights into the immediate rearrangements of the chromophore and surrounding residues (Table S3). Following chromophore isomerization, the interactions between the chromophore and the residues in its vicinity are heavily remodeled (Fig. 3C). The pocket around BV can be divided into three main spatial interfaces. Firstly, a number of highly conserved residues stabilize the BV in the pocket through hydrogen bonding and electrostatic interactions. Most prominently, R254, Y216, H260, S272, and S274 (*Deinococcus radiodurans* BphP (DrBphP) [126] numbering used further on) stabilize the two propionic acid substituents on ring B and C. Additionally the backbone of D207 interacts in a coordinating fashion with the nitrogens of rings A to C. Secondly, the residues lining the D-ring provide the stage for the isomerization. High-resolution structures show that the D-ring of BV has considerably more freedom to move within the pocket than the other pyrrole rings [127,128]. Lastly, the highly conserved PRxSF motif in the PHY tongue and the DIP motif in the GAF domain form the interaction interface required for the conformational relay upon photoswitching.

An extensive stabilizing hydrogen network is rearranged after chromophore isomerization, as confirmed by ^{1}H–^{13}C magic-angle spinning NMR [129]. In the *cis* state, H290 interacts with the D-ring carbonyl and in the *trans* state, D207 and Y263 form a network with the D-ring carbonyl and nitrogen. Those residues serve as the essential connectors between chromophore isomerization and the protein. Interestingly, a few consistent water molecules are present in close contact with the chromophore and within H-bond distance to D207, Y263, and H290, hinting at a role in photoconversion that has not been fully clarified to date [127,128,130]. In the *cis* state, the interaction with H290 effectively keeps the D-ring out of the interaction reach of D207 and Y263, making them available to interact with R466 in the 'PHY tongue' [131], which consequently adopts a β-hairpin conformation.

In contrast, the re-positioned D-ring in the *trans* conformation can interact with D207 and Y263, altering their spatial position and replacing their interactions with R466 to S468 instead [132]. This exchange induces a conformational switch in the PHY tongue from a β-hairpin to an α-helix. The stabilizing function of the 'PHY tongue' residues on the *trans* chromophore is exemplified by engineered BphP variants lacking the PHY domain: these variants show more than 100 times faster dark relaxation to P_r [128,133]. In agreement, P465 and F469 form an interaction interface with a helix in the GAF domain, providing a hydrophobic environment that stabilizes the *trans* state [134-136]. Of note, an F469W mutation further stabilizes the *trans* P_{fr} state by severely slowing down dark relaxation back to the *cis* P_r state [136].

Photoswitching-induced structural remodeling: PHY tongue refolding and long-range conformational relay

As detailed above, the refolding of the PHY tongue upon photoconversion is the trigger for the subsequent conformational changes along the BphP protein, which ultimately lead to the activation of the downstream effector domain. Although the relay system within the PCM is highly conserved, there are significant variations in the conformational relay mechanism between PCM and OPM. This agrees with the functional and structural diversity that the OPM module can have. Typically, the P_{fr} state with the *trans* chromophore has the highest catalytic activity; however, there are exceptions where red illumination actually inhibits activity, such as in bathy Agp2 [137], the *Bradyrhizobium* BphP [138], and *Rhodopseudomonas palustris* RpBphP1 [139], as well as in constitutively active proteins RpBphP2

[140] and Agp1 [100]. The current consensus model for full-length BphPs agrees that the tighter PHY-GAF interaction and PHY tongue refolding create a strain in the 'helical spine'. The dimer helices composing the spine are packed in a parallel coiled-coil bundle, which due to the imposed strain, twists around its axis by 50°, with a rotation of the dimer OPMs in relation to the PSMs (Fig. 3D). The OPM-PSM relative rotation has been observed in full-length structures of several phytochromes [141–144], as well as in other sensors containing HK and cyclase domains [145–147]. In fact, the spine twisting mechanism is so robust that it occurs even when only one homodimer sub-unit is asymmetrically activated, leading to the formation of a heterodimer of the protein photo-states [144]. However, recently published cryo-EM structures of full-length DrBphP revealed an alternative zipper-like opening (instead of twisting) of the OPM-dimeric spine helices, which still leads to a stark repositioning of the OPMs [148]. Thus consensually, the coiled-coil spine appears to be the critical transducer for BphP functional activation. The structures from IsPadC (phytochrome activated diguanylyl cyclase from *Idiomarina species A28L*) provide evidence that the coiled-coil spine has two distinct registers: one for the protein's resting state and another for the red light-activated state, which is unlocked upon the spine's rotation [143,144]. The length of the PHY-OPM helix can vary by heptads of amino acids; each heptad is around two full α-helix turns, conserving the relative orientation of OPM and PSM. The specific amino acid composition of these heptads not only fine-tunes the strength of the dimerization interface but, most importantly, tailors the OPM activation dynamics *via* the rotational switch between spine registers. In IsPadC activation studies, when the spine was mutated to stabilize the resting register, the protein could no longer be activated by red light; alternatively, stabilization of the red light-illuminated register led to a constantly active IsPadC [143]. This regulatory model based on coiled-coil heptad length and configuration switch is in line with the coiled-coil linker regulation observed in various proteins with HK [149–151] and diguanylate cyclase domains [152,153]—both common BphPs output effectors. The recently discovered model of zipper-like opening of the dimeric spine helices is in line with heptad length regulation but apparently independent of the two-helix register activation [148]. However, BphPs truncated to their PCM show a stark variation from the above consensus model. Due to the lack of the OPM (and probably an incomplete dimer interface), the activated PHY-GAF-induced strain leads to a breakage of the PHY-OPM dimer interface, the spine

helices bend relative to one another, repositioning the PHY domain and opening an inner 'cavity' within the BphP dimer [128,154,155]. Interestingly, changes in the modular organization of BphPs can alter their conformational relay mechanism and quaternary structure. For example, RpBphP1 (domain organization PAS-GAF-PHY-PAS/PAC-HOS) forms parallel head-to-head homodimers in the dark P_{fr} state, but changes into an antiparallel heterodimer with its functional partner RpPpsR2 in the P_r state, when exposed to far-red light [156]. The homodimer dissolution is proposed to occur when the far-red light-induced loss of interaction between the HOS domain and the GAF-PHY helix results in the release of the former, making it available to bind to RpPpsR2, with the concurrent disruption of the homodimer interface. Another notable example is XccBphP from *Xanthomonas campestris* (domain organization PAS-GAF-PHY-PAS9) in which the red light-induced PHY tongue refolding pulls on the spine helix in a way that causes it to straighten, leading to loss of the dimer interfaces and consequent monomerization. In this transient monomer state, the PHY-OPM helix is able to bend halfway by 90°, repositioning the PAS9 domain to form a C-shape monomer that ultimately flips the two molecules into a head-to-tail dimer in the P_{fr} state [157].

In summary, the biological activity of BphPs is activated through a cascade of conformational changes initiated by light-driven chromophore isomerization. This cascade comprises defined triggers that exist in an equilibrium between two states: *cis* vs. *trans* chromophore, β-sheet vs. α-helix PHY tongue, and resting vs. active spine configuration.

Different BphPs fine-tune their biological response by modifications in their protein matrix, which affect the equilibria mentioned above. For instance, mutations in the chromophore pocket can alter dark reversion times [136] or different coiled-coil spine length can alter the activity of effector domains [158]. However, the directionality of the equilibria is the same—from photoisomerization to downstream allosteric OPM activation. The reverse 'upstream' direction—how protein matrix changes can influence the spectral properties of a BphP—is still largely unexplored. A DrBphP variant with the Y263F mutation provided initial evidence for this bidirectional influence. This mutation results in a less-stabilized P_{fr}, with an increased fluorescence quantum yield at the expense of isomerization upon red light illumination; strikingly, the quaternary structure was that of the P_{fr} state as the PHY tongue was locked in the P_{fr} α-helix conformation. The Y263 residue works simultaneously to support the isomerization and to stabilize the GAF-

PHY tongue interaction and hence is crucial in coupling both processes [159]. Recently, two studies systematically tested the influence of the protein matrix on the photophysics and output activity, by building chimeras of two BphPs: IsPadC and TsPadC [160], as well as IsPadC and MpPadC, respectively. The subsequent comparative analysis supported the bidirectionality of coupled equilibria with tunable interdependencies. For example, changes in the PCM components, particularly in the PHY tongue region and an N-terminal segment (NTS) (residues 1–16), led to altered spectral profiles and OPM activity. The PHY-OPM helix was crucial for activity regulation as expected, but in some instances, could also influence the spectral profile. As so, such an engineering approach could be harnessed to produce BphP chimeric variants that have a range of spectral profiles and activity modes. Indeed, while the native BphP light-signal relay system has been employed in optogenetics, the protein matrix engineering to change BphP photophysics has been increasingly explored in the fields of NIR-FPs and, more recently, biosensors.

Engineering of optogenetic tools based on BphPs

The unique modularity of BphPs and their ability to transduce light signals into long-range conformational changes are exploited to develop optogenetic tools by engineering chimeras between the PCM and an effector module of choice. This review focuses on the structural requirements to build BphP-based optogenetic tools as their individual characteristics and applications have been comprehensively reviewed, e.g., by Shcherbakova *et al.* [161]. The most intuitive site to target when building chimeras is the α-helix protruding from the PHY domain into the OPM (Fig. 3F, marked 1). Together with the GAF-PHY helix, this PHY-OPM helix forms the BphP 'helical spine', a part of the photoswitching structural relay system. The modularity of these proteins makes it simple to swap domains from different BphPs, pairing a BphP with desirable photophysical characteristics with a catalytic domain of another suited for the desired function. An example of this approach is the photoactivated synthesis of cyclic dimeric GMP (c-di-GMP) generated by exchanging between different diguanylate cyclase OPM domains [162].

Another intuitive approach is to swap BphP OPM domains with other protein domains of similar fold. In an engineered red light-activated phosphodiesterase (PDE), the PDE domain of the human protein HsPDE2A is truncated at the junction with an α-helix of an upstream GAF domain and attached to the last

helix exiting the PHY domain of BphP [163]. The chimera is facilitated by the fact that both parts—the upstream GAF of HsPDE2A and the BphP PHY— share the same GAF domain-like fold (α-β(2)-α(n)-β (3)-alpha, antiparallel β-sheet). A more complex option is to replace the OPM with a structurally different domain. In a red light-regulated adenylate cyclase (AC), the diguanylate cyclase OPM of the *Rhodobacter sphaeroides* BphG1 was exchanged by an AC domain, which is only active as a homodimer. The study concluded that the merging positions on the PHY-OPM helix able to maintain AC dimerization and light sensitivity all kept a compatible helix register plus a 11–22 Å distance between helices in the photoactivated state, and a > 40 Å distance between AC domains in the inactive state [158]. Thus, in such engineered constructs, the key determinants for achieving light-regulated activity are the length and register of the PHY-OPM helix, which control the distance and rotation between the two helices, and thus the alignment of the OPMs.

Lastly, the light-regulated quaternary structure rearrangements of BphPs can also be harnessed in the development of optogenetics tools. In two different NIR-activated receptor tyrosine kinases (RTKs), the PCM of DrBphP replaced the extracellular and transmembrane domains of the RTKs while their native cytoplasmic domain was kept. Native RTKs are inactive when monomeric and require activation by extracellular signaling which induces their dimerization. In the engineered NIR-regulated RTK, the compact structure of the P_r state PCM homodimer mimics the dimeric state of the RTK and activates the protein in response to far-red light. Conversely, the open conformation of the P_{fr} state homodimer separates the cytoplasmic domains, imitating the inactive RTK monomer [164]. Similarly, one of the first optogenetic systems based on BphPs explored the atypical heterodimerization mechanism between RpBphP1 and PspR2 of *R. palustris*. Upon NIR-light activation, conformational changes from the P_r state lead to the dissociation of the RpBphP1 homodimer and the formation of RpBphP1 / PspR2 heterodimers. Thus, this system can be employed for the light-dependent recruitment of different proteins leading to different cellular responses (e.g., cytoskeletal rearrangement or transcriptional activation) [165].

Use of the reversible photoswitching of BphPs in fluorescence imaging

Despite their non-fluorescent native form, several modifications have been introduced in BphPs, producing

engineered FPs with great potential for tissue imaging. Their excitation and emission ranges are at WL beyond 650 nm ('optical window' ~ 650 nm - 900 nm) which increases penetration depth and decreases scattering. Fluorescence emission is detected from the P_r state excitation; thus, de-excitation of the chromophore *via* fluorescence is in direct competition with the P_r to P_{fr} transition, effectively reducing the fluorescence signal. Hence to obtain permanent and bright fluorescence, the first step is to truncate the protein to the minimal PAS-GAF domains (Fig. 3F, marked 2), or even just GAF [166] domains, which consequently destabilizes the P_{fr} state, disables photoconversion and any downstream effects. Subsequent optimization involves mutagenesis of the surrounding pocket residues to form a hydrogen bond network with *cis* BV, stabilizing the P_r state. Essentially all fluorescent nonswitching variants of BphPs show mutations in D207 and/or Y263 (Y263: WiPhy, SNIFP; D207: IRFPs). For excellent overviews on nonphotoswitching BphPs for fluorescence imaging, see references by Shcherbakova *et al.* and Oliinyk *et al.* [7,97,167]. From the imaging perspective, fluorescent BphPs extend the spectral palette to the NIR, e.g., for deeper penetration in scattering media (tissue) or to avoid spectral overlap. Although their fluorescence quantum yields are relatively low, they are comparable to those of far-red GFP-like FPs (Table S1). For some BphPs this is alleviated by higher extinction coefficients (e.g., SNIFP with 150 000 M^{-1} cm^{-1}). However, the necessity for the prosthetic BV chromophore might jeopardize cellular brightness, in cases of competition for BV or hampered chromophorylation. Fluorescent BphPs are on par with GFP-like FPs regarding ease of labeling and toxicity, allowing for straight forward application [168]. While systematic comparisons of photofatigue are lacking, a comparison of SNIF and emiRFP703 with several far-red GFP-like proteins shows comparable behavior, with BphPs tending to higher photostability [169]. The dimeric behavior of BphPs poses a potential drawback for subcellular imaging of protein fusions, although several monomer variants have been created. In many aspects, the developments and initiatives involving fluorescent BphP-based proteins are comparable with the advent of GFP-like proteins.

Use of the reversible photoswitching of BphPs in optoacoustic imaging

Recently, the use of BphPs with their native photoswitching functionality gained attention in imaging, particularly in optoacoustic imaging (OA) also known as photoacoustic imaging. OA is a unique modality for *in vivo* in-tissue imaging using light excitation and ultrasound detection. This combination allows for the versatility of optical excitation for contrast, while circumventing the detection problem inherent to methods that use light for both excitation and detection (namely low penetration depth due to scattering in detection). While OA is firmly establishing itself in biomedical imaging [170–173], its full potential in the life sciences has been so far limited by the lack of suitable genetically encodable contrast agents. The main challenge is that any contrast agent needs to compete against the massive background of hemoglobin present in the blood. Here, photoswitching BphPs can be used to modulate the signal and separate it from the nonswitching background, making it virtually invisible.

Several BphPs have been used in OA approaches with RpBphP1 being the subject of the first study that probed its nonfluorescent P_{fr} state vs. its P_r state during repeated switching cycles in a differential imaging approach. RpBphP1 showed enhanced sensitivity and background suppression compared with nonswitching agents, when imaging tumors at a depth close to 10 mm [174]. The truncation to the PCM domain is favorable as it reduces the size of the protein (relevant for ease of transfection, etc.), but it however needs to preserve the protein's photoswitching capabilities. In this regard, the protein sGPC2 was engineered from a single GAF domain of the BV-binding cyanobacteriochrome of *Acaryochloris marina*, to be photoswitchable despite being only 16.8 kDa, making it around a quarter of other developed BphP-PCMs [175]. However, sGPC2's maximum absorption is blue-shifted (P_r peak at 630 nm and P_{fr} at 700 nm), potentially hindering tissue penetration. Fast acquisition ideally relies on BphPs with fast transitions and low photofatigue. The switching kinetics can be accelerated by mutating the PRxSF motif in the PHY tongue. For example, a DrBphP-PCM variant with an F469W mutation delays dark relaxation and favors the P_r to P_{fr} transition, with a P_{fr} population of ~ 87% after photoconversion [136]. This results in an improved photoswitching contrast during imaging, as the increased P_{fr} quantum yield, together with proper P_{fr} to P_r back conversion, leads to an increase in the signal differential when compared to wild-type DrBphP and RpBphP1 [176]. Another study found that a BphP from *Rhizobium etli* (ReBphP) [104], truncated to its minimal PCM, showed nearly four times faster switching compared with DrBphP-PCM and RpBphP1 [177]. This effect is likely due to an additional arginine in the PHY tongue (not present in DrBphP or RpBphP1), which directly interacts with a conserved aspartate in the GAF domain (Asp207 in DrBphP), lowering P_{fr} stabilization from the serine in the PRxSF motif.

The different photoswitching speeds of BphPs have allowed for multiplexing approaches using exponential fits to distinguish labeled cell populations [177,178]; a concept similar to the unmixing based on switching kinetics described above for RSFPs. Recently, the application of photoswitching BphPs as genetically encoded probes for enhanced optoacoustic contrast reached a new level of maturity. The firstly developed transgenic *loxP-RpBphP1* mouse model allowed for specific and regulated RpBphP1 expression and imaging by OA tomography in various tissues [179].

Returning to ReBphP, the results of the PCM truncation study itself are of particular interest since they showed that including part of the PHY-OPM helix is required to achieve a maximum P_{fr}/P_r population photoconversion [177]. Since the variant is a monomer in solution, the effect cannot be attributed to changes in the dimer conformation (as described above). This suggests a bidirectional link between protein photophysics and structure: not only is the photo-induced tongue refolding required for PHY-OPM helix rotation, but the presence of the helix may also be needed for PHY refolding to stabilize the photo-states of the chromophore. This possibility is especially relevant for the development of BphP-based sensors, where the signal relay in the opposite direction from the sensing domain (the OPM-replacing domain) to PCM—is also required opposite direction.

Sensors based on BphPs

The far-red absorbance and fluorescence of BphPs provide strong advantages for imaging. Hence, it is not surprising that developments also include their use in molecular sensors for small molecules and ions. Similar concepts as those used for GFP-based sensors have started to emerge for BphPs. For example, a Förster resonance energy transfer (FRET)-based sensor for Rac1 GTPase activity was built using BphPs mIRFP720 and mIRFP670 [180]; similarly, a BphP-based calcium sensor was built (iGECI) with a related FRET pair [181]. Chimeric sensors based on a single BphP are capable of directly harnessing chromophore interactions to relay ligand-binding. While the field of chimeric GFP-based sensors has benefited by the advent of cpGFP [81] (see above), there is currently no equivalent concept for BphPs. So far, only a mapping of potential permutation sites for new N- and C-termini has been conducted by analyzing a circularly permuted iRFP (only PAS-GAF domains) library for fluorescence and expression [182]. Covering 58% of possible permutations, the authors found 27 fluorescent variants whose new N- and C-termini were

primarily at the linker between the PAS and GAF domain (residue ~ 100–150) and the previous N-terminal region (< 19, Fig. 3F, marked 3). From these, 5 circularly permuted variants maintained or exceeded iRFP fluorescence but only the entry sites 12 and 133 (iRFP numbering) showed expression levels suitable for application in mammalian cells. The circularly permuted position 12 might be promising due to its placement at the flank of the NTS, a region coupling the chromophore isomerization and large-scale conformational change [160], and due to its closeness to the BV-pocket. A more basic sensor engineering strategy is to insert the entire readout moiety, with its normal N- and C-termini, at different positions in the BphP (Fig. 3E). As of now, two entry sites have been chosen from whose different conclusions on the interplay with the chromophore can be extracted. One entry site is within the first loop of the GAF domain β-sheet (180, Fig. 3F marked 4). In fact, calcium sensors were built by inserting a Calmodulin/RS20 fusion into this site in mIFP [93,183]. Also, a blue-shifted version (~ 40 nm) of this sensor class has been produced by adding a second cysteine in the binding pocket creating two thioether linkages and thus shortening the π-electron system [184]. The second entry site is found at the beginning of the α-helix enclosing the chromophore at the opposite side from the β-sheet (258, Fig. 3F, marked 5) [94,185]. At the other end of this α-helix lies the P_{fr}-stabilizing Y263, which interacts with the chromophore and is removed in many engineered non-switching BphPs but maintained in these constructs despite their nonswitchability. Thus, it might be possible that slight positional changes due to the movement of the helix because of the attached receptor moiety are relayed to the chromophore through Y263. So far, the only sensor preserving the native BphP photoswitching is a protein-fragment complementation assay-based sensor concept called DrSplit [178]. It is based on the DrBphP-PCM split between PAS (BV attaching thioester cysteine) and GAF domains (main BV-binding pocket) fused to two interacting protein fragments. Only reconstitution of both parts allows chromophore attachment and thus functional photoswitching and signal generation.

Outlook

The direct relay between protein structure and chromophore is one of the most fascinating aspects of protein functionality. Based on the examples from two classes—RSFPs and BphPs—we highlight the bidirectional nature of this interplay. That is, how a light-induced chromophore isomerization can immediately reshape

the vicinity of the chromophore-surrounding protein matrix but ultimately lead to long-ranging conformational changes, ranging from secondary structure changes to domain rearrangement and oligomerization switches. In the reverse direction, the protein matrix itself can shape the chromophore photophysics, once again ranging from the local influence of the chromophore-neighboring residues to distant upstream changes that are structurally relayed to the chromophore environment. While present research and developments on BphPs covered the former directionality more extensively, the latter directionality is largely represented in FP sensors and RSFPs photophysical engineering.

For RSFPs, also due to the limited degrees of freedom of the β-barrel, the protein matrix influence on the chromophore isomerization is mainly exerted *via* a number of residues, especially in β-strands 7 and 8. By contrast, the downstream effector path in BphPs (from chromophore-photon absorption to output domain activation) relies on the sequential signal relay from local residues to distant structural elements. While the downstream path has been thoroughly dissected and its parts characterized, the upstream relay system (from conformational changes to chromophore photophysics) has only very recently been harnessed in the context of sensor engineering, as shown in BphP-based calcium sensors. Thus, there are many interesting possibilities, for instance, taking advantage of a general 'upstream' relay path that remains to be investigated. It remains to be seen if this transduction system can follow the same steps as the 'downstream' path (i.e., alterations of the isomerization state or photoswitching photophysics due to structural rearrangements exerted on the PHY-OPM helix) and to which extent these coupled states can be tweaked and utilized in applications. In FPs, an example of what could be considered an 'upstream relay path' is the pH-induced chromophore isomerization observed in mKate, in the absence of light. In the future, it would be interesting to expand on this concept and test whether it is possible to achieve non-light-induced chromophore isomerization through a relay of residue rearrangements in the surrounding pocket. Here, BphPs offer an evident versatility with which FPs cannot compete, first due to their native structural modularity. Second, the well-characterized chromophore-to-structure relay steps are starting points to investigate the reverse structure-to-chromophore transduction.

Acknowledgements

References

1 Emiliani V, Entcheva E, Hedrich R, Hegemann P, Konrad KR, Lüscher C, Mahn M, Pan ZH, Sims RR, Vierock J *et al.* (2022) Optogenetics for light control of biological systems. *Nat Rev Methods Primers* **2**, 55.

2 Deisseroth K, Feng G, Majewska AK, Miesenböck G, Ting A and Schnitzer MJ (2006) Next-generation optical technologies for illuminating genetically targeted brain circuits. *J Neurosci* **26**, 10380–10386.

3 Schneider F, Grimm C and Hegemann P (2015) Biophysics of channelrhodopsin. *Annu Rev Biophys* **44**, 167–186.

4 Tye KM and Deisseroth K (2012) Optogenetic investigation of neural circuits underlying brain disease in animal models. *Nat Rev Neurosci* **13**, 251–266.

5 Goto Y, Kondo Y and Aoki K (2021) Visualization and manipulation of intracellular signaling. *Adv Exp Med Biol* **1293**, 225–234.

6 Tsien RY (1998) The green fluorescent protein. *Annu Rev Biochem* **67**, 509–544.

7 Oliinyk OS, Chernov KG and Verkhusha VV (2017) Bacterial phytochromes, cyanobacteriochromes and allophycocyanins as a source of near-infrared fluorescent probes. *Int J Mol Sci* **18**, 1691.

8 Buckley AM, Petersen J, Roe AJ, Douce GR and Christie JM (2015) LOV-based reporters for fluorescence imaging. *Curr Opin Chem Biol* **27**, 39–45.

9 Bond C, Santiago-Ruiz AN, Tang Q and Lakadamyali M (2022) Technological advances in super-resolution microscopy to study cellular processes. *Mol Cell* **82**, 315–332.

10 Liu S, Hoess P and Ries J (2022) Super-resolution microscopy for structural cell biology. *Annu Rev Biophys* **51**, 301–326.

11 Barykina N v, Karasev MM, Verkhusha V v and Shcherbakova DM (2022) Technologies for large-scale mapping of functional neural circuits active during a user-defined time window. *Prog Neurobiol* **216**, 102290.

12 Ebner C, Ledderose J, Zolnik TA, Dominiak SE, Turko P, Papoutsi A, Poirazi P, Eickholt BJ, Vida I,

Larkum ME *et al.* (2019) Optically induced calcium-dependent gene activation and labeling of active neurons using CaMPARI and Cal-light. *Front Synaptic Neurosci* **11**, 16.

13 Mishra K, Fuenzalida-Werner JP, Ntziachristos V and Stiel AC (2019) Photocontrollable proteins for optoacoustic imaging. *Anal Chem* **91**, 5470–5477.

14 Chouket R, Pellissier-Tanon A, Lahlou A, Zhang R, Kim D, Plamont MA, Zhang M, Zhang X, Xu P, Desprat N *et al.* (2022) Extra kinetic dimensions for label discrimination. *Nat Commun* **13**, 1482.

15 Eggeling C, Willig KI, Sahl SJ and Hell SW (2015) Lens-based fluorescence nanoscopy. *Q Rev Biophys* **48**, 178–243.

16 Sahl SJ and Moerner WE (2013) Super-resolution fluorescence imaging with single molecules. *Curr Opin Struct Biol* **23**, 778–787.

17 Egner A, Geisler C, von Middendorff C, Bock H, Wenzel D, Medda R, Andresen M, Stiel AC, Jakobs S, Eggeling C *et al.* (2007) Fluorescence nanoscopy in whole cells by asynchronous localization of photoswitching emitters. *Biophys J* **93**, 3285–3290.

18 Qian Y, Celiker OT, Wang Z, Guner-Ataman B and Boyden ES (2022) Temporally multiplexed imaging of dynamic signaling networks in living cells. *bioRxiv* doi: 10.1101/2022.08.22.504781

19 Lambert TJ (2019) FPbase: a community-editable fluorescent protein database. *Nat Methods* **16**, 277–278.

20 Stiel AC, Andresen M, Bock H, Hilbert M, Schilde J, Schönle A, Eggeling C, Egner A, Hell SW and Jakobs S (2008) Generation of monomeric reversibly switchable red fluorescent proteins for far-field fluorescence nanoscopy. *Biophys J* **95**, 2989–2997.

21 Bui TYH, Moeyaert B, Pecqueur L, Srinivasu B, Economou A, Fontecave M, Dedecker P and van Meervelt L (2021) Structural evidence for the bleaching caused by oxygen in rsCherry. *Acta Crystallogr* **A77**, C343.

22 Pennacchietti F, Serebrovskaya EO, Faro AR, Shemyakina II, Bozhanova NG, Kotlobay AA, Gurskaya NG, Bodén A, Dreier J, Chudakov DM *et al.* (2018) Fast reversibly photoswitching red fluorescent proteins for live-cell RESOLFT nanoscopy. *Nat Methods* **15**, 601–604.

23 Bourgeois D (2017) Deciphering structural photophysics of fluorescent proteins by kinetic crystallography. *Int J Mol Sci* **18**, 1187.

24 Loos DC, Habuchi S, Flors C, Hotta JI, Wiedenmann J, Nienhaus GU and Hofkens J (2006) Photoconversion in the red fluorescent protein from the sea anemone Entacmaea quadricolor: is cis-trans isomerization involved? *J Am Chem Soc* **128**, 6270–6271.

25 Jung YO, Lee JH, Kim J, Schmidt M, Moffat K, Šrajer V and Ihee H (2013) Volume-conserving trans–cis isomerization pathways in photoactive yellow protein visualized by picosecond X-ray crystallography. *Nat Chem* **5**, 212–220.

26 Liu RSH (2001) Photoisomerization by hula-twist: a fundamental supramolecular photochemical reaction. *Acc Chem Res* **34**, 555–562.

27 Gerwien A, Schildhauer M, Thumser S, Mayer P and Dube H (2018) Direct evidence for hula twist and single-bond rotation photoproducts. *Nat Commun* **9**, 2510.

28 Duan C, Adam V, Byrdin M and Bourgeois D (2014) Structural basis of photoswitching in fluorescent proteins. *Methods Mol Biol* **1148**, 177–202.

29 Pletnev S, Shcherbo D, Chudakov DM, Pletneva N, Merzlyak EM, Wlodawer A, Dauter Z and Pletnev V (2008) A crystallographic study of bright far-red fluorescent protein mKate reveals pH-induced cis-trans isomerization of the chromophore. *J Biol Chem* **283**, 28980–28987.

30 Christou NE, Giandoreggio-Barranco K, Ayala I, Glushonkov O, Adam V, Bourgeois D and Brutscher B (2021) Disentangling chromophore states in a reversibly switchable green fluorescent protein: mechanistic insights from NMR spectroscopy. *J Am Chem Soc* **143**, 7521–7530.

31 Habuchi S, Dedecker P, Hotta JI, Flors C, Ando R, Mizuno H, Miyawaki A and Hofkens J (2006) Photo-induced protonation/deprotonation in the GFP-like fluorescent protein Dronpa: mechanism responsible for the reversible photoswitching. *Photochem Photobiol Sci* **5**, 567–576.

32 Brakemann T, Stiel AC, Weber G, Andresen M, Testa I, Grotjohann T, Leutenegger M, Plessmann U, Urlaub H, Eggeling C *et al.* (2011) A reversibly photoswitchable GFP-like protein with fluorescence excitation decoupled from switching. *Nat Biotechnol* **29**, 942–947.

33 Lambert GG, Depernet H, Gotthard G, Schultz DT, Navizet I, Lambert T, Adams SR, Torreblanca-Zanca A, Chu M, Bindels DS *et al.* (2020) Aequorea's secrets revealed: new fluorescent proteins with unique properties for bioimaging and biosensing. *PLoS Biol* **18**, e3000936.

34 Niwa H, Inouye S, Hirano T, Matsuno T, Kojima S, Kubota M, Ohashi M and Tsuji FI (1996) Chemical nature of the light emitter of the *Aequorea* green fluorescent protein. *Proc Natl Acad Sci* **93**, 13617–13622.

35 Voliani V, Bizzarri R, Nifosì R, Abbruzzetti S, Grandi E, Viappiani C and Beltram F (2008) Cis − Trans photoisomerization of fluorescent-protein chromophores. *J Phys Chem B* **112**, 10714–10722.

36 Jung G, Bräuchle C and Zumbusch A (2001) Two-color fluorescence correlation spectroscopy of one chromophore: application to the E222Q mutant of the

green fluorescent protein. *J Chem Phys* **114**, 3149–3156.

37 Romei MG, Lin C-Y, Mathews II and Boxer SG (2020) Electrostatic control of photoisomerization pathways in proteins. *Science* **367**, 76–79.

38 Scharnagl C and Raupp-Kossmann RA (2004) Solution pK_a values of the green fluorescent protein chromophore from hybrid quantum-classical calculations. *J Phys Chem B* **108**, 477–489.

39 Brakemann T, Weber G, Andresen M, Groenhof G, Stiel AC, Trowitzsch S, Eggeling C, Grubmüller H, Hell SW, Wahl MC et al. (2010) Molecular basis of the light-driven switching of the photochromic fluorescent protein Padron. *J Biol Chem* **285**, 14603–14609.

40 de Zitter E, Hugelier S, Duwé S, Vandenberg W, Tebo AG, van Meervelt L and Dedecker P (2021) Structure–function dataset reveals environment effects within a fluorescent protein model system. *Angew Chem Int Ed* **60**, 10073–10081.

41 Morozov D and Groenhof G (2016) Hydrogen bond fluctuations control photochromism in a reversibly photo-switchable fluorescent protein. *Angew Chem Int Ed Engl* **128**, 586–588.

42 Rocha S, de Keersmaecker H, Uji-i H, Hofkens J and Mizuno H (2014) Photoswitchable fluorescent proteins for superresolution fluorescence microscopy circumventing the diffraction limit of light. *Methods Mol Biol* **1076**, 793–812.

43 Stiel AC, Trowitzsch S, Weber G, Andresen M, Eggeling C, Hell SW, Jakobs S and Wahl MC (2007) 1.8 A bright-state structure of the reversibly switchable fluorescent protein Dronpa guides the generation of fast switching variants. *Biochem J* **402**, 35–42.

44 Ando R, Flors C, Mizuno H, Hofkens J and Miyawaki A (2007) Highlighted generation of fluorescence signals using simultaneous two-color irradiation on Dronpa mutants. *Biophys J* **92**, L97–L99.

45 Ando R, Mizuno H and Miyawaki A (2004) Regulated fast nucleocytoplasmic shuttling observed by reversible protein highlighting. *Science* **306**, 1370–1373.

46 Bourgeois D and Adam V (2012) Reversible photoswitching in fluorescent proteins: a mechanistic view. *IUBMB Life* **64**, 482–491.

47 Tang L and Fang C (2022) Photoswitchable fluorescent proteins: mechanisms on ultrafast timescales. *Int J Mol Sci* **23**, 6459.

48 Acharya A, Bogdanov AM, Grigorenko BL, Bravaya KB, Nemukhin AV, Lukyanov KA and Krylov AI (2017) Photoinduced chemistry in fluorescent proteins: curse or blessing? *Chem Rev* **117**, 758–795.

49 Shcherbakova DM and Verkhusha VV (2014) Chromophore chemistry of fluorescent proteins controlled by light. *Curr Opin Chem Biol* **20**, 60–68.

50 Uriarte LM, Vitale R, Niziński S, Hadjidemetriou K, Zala N, Lukacs A, Greetham GM, Sazanovich IV, Weik M, Ruckebusch C et al. (2022) Structural information about the trans-to- cis isomerization mechanism of the photoswitchable fluorescent protein rsEGFP2 revealed by multiscale infrared transient absorption. *J Phys Chem Lett* **13**, 1194–1202.

51 Woodhouse J, Nass Kovacs G, Coquelle N, Uriarte LM, Adam V, Barends TRM, Byrdin M, de la Mora E, Bruce Doak R, Feliks M et al. (2020) Photoswitching mechanism of a fluorescent protein revealed by time-resolved crystallography and transient absorption spectroscopy. *Nat Commun* **11**, 741.

52 Coquelle N, Sliwa M, Woodhouse J, Schirò G, Adam V, Aquila A, Barends TRM, Boutet S, Byrdin M, Carbajo S et al. (2018) Chromophore twisting in the excited state of a photoswitchable fluorescent protein captured by time-resolved serial femtosecond crystallography. *Nat Chem* **10**, 31–37.

53 Andresen M, Stiel AC, Trowitzsch S, Weber G, Eggeling C, Wahl MC, Hell SW and Jakobs S (2007) Structural basis for reversible photoswitching in Dronpa. *Proc Natl Acad Sci U S A* **104**, 13005–13009.

54 Zhang X, Zhang M, Li D, He W, Peng J, Betzig E and Xu P (2016) Highly photostable, reversibly photoswitchable fluorescent protein with high contrast ratio for live-cell superresolution microscopy. *Proc Natl Acad Sci U S A* **113**, 10364–10369.

55 el Khatib M, Martins A, Bourgeois D, Colletier J-P and Adam V (2016) Rational design of ultrastable and reversibly photoswitchable fluorescent proteins for super-resolution imaging of the bacterial periplasm. *Sci Rep* **6**, 18459.

56 Andresen M, Wahl MC, Stiel AC, Gräter F, Schäfer LV, Trowitzsch S, Weber G, Eggeling C, Grubmüller H, Hell SW et al. (2005) Structure and mechanism of the reversible photoswitch of a fluorescent protein. *Proc Natl Acad Sci U S A* **102**, 13070–13074.

57 Schäfer LV, Groenhof G, Boggio-Pasqua M, Robb MA and Grubmüller H (2008) Chromophore protonation state controls photoswitching of the fluoroprotein asFP595. *PLoS Comput Biol* **4**, e1000034.

58 Schäfer LV, Groenhof G, Klingen AR, Ullmann GM, Boggio-Pasqua M, Robb MA and Grubmüller H (2007) Photoswitching of the fluorescent protein asFP595: mechanism, proton pathways, and absorption spectra. *Angew Chem Int Ed Engl* **119**, 536–542.

59 Regis Faro A, Carpentier P, Jonasson G, Pompidor G, Arcizet D, Demachy I and Bourgeois D (2011) Low-temperature chromophore isomerization reveals the photoswitching mechanism of the fluorescent protein Padron. *J Am Chem Soc* **133**, 16362–16365.

60 Mizuno H, Mal TK, Wälchli M, Kikuchi A, Fukano T, Ando R, Jeyakanthan J, Taka J, Shiro Y, Ikura M et al. (2008) Light-dependent regulation of structural flexibility in a photochromic fluorescent protein. *Proc Natl Acad Sci U S A* **105**, 9227–9232.

61 Mizuno H, Mal TK, Wälchli M, Fukano T, Ikura M and Miyawaki A (2010) Molecular basis of photochromism of a fluorescent protein revealed by direct 13C detection under laser illumination. *J Biomol NMR* **48**, 237–246.

62 Seifert MHJ, Georgescu J, Ksiazek D, Smialowski P, Rehm T, Steipe B and Holak TA (2003) Backbone dynamics of green fluorescent protein and the effect of histidine 148 substitution. *Biochemistry* **42**, 2500–2512.

63 Kao Y-TT, Zhu X and Min W (2012) Protein-flexibility mediated coupling between photoswitching kinetics and surrounding viscosity of a photochromic fluorescent protein. *Proc Natl Acad Sci U S A* **109**, 3220–3225.

64 Adam V, Hadjidemetriou K, Jensen N, Shoeman RL, Woodhouse J, Aquila A, Banneville AS, Barends TRM, Bezchastnov V, Boutet S et al. (2022) Rational control of off-state heterogeneity in a photoswitchable fluorescent protein provides switching contrast enhancement. *ChemPhysChem* **23**, e202200192.

65 Chang J, Romei MG and Boxer SG (2019) Structural evidence of photoisomerization pathways in fluorescent proteins. *J Am Chem Soc* **141**, 15504–15508.

66 Christou NE, Ayala I, Giandoreggio-Barranco K, Byrdin M, Adam V, Bourgeois D and Brutscher B (2019) NMR reveals light-induced changes in the dynamics of a photoswitchable fluorescent protein. *Biophys J* **117**, 2087–2100.

67 Pozzi EA, Schwall LR, Jimenez R and Weber JM (2012) Pressure-induced changes in the fluorescence behavior of red fluorescent proteins. *J Phys Chem B* **116**, 10311–10316.

68 Laurent AD, Mironov VA, Chapagain PP, Nemukhin A v and Krylov AI (2012) Exploring structural and optical properties of fluorescent proteins by squeezing: modeling high-pressure effects on the mStrawberry and mCherry red fluorescent proteins. *J Phys Chem B* **116**, 12426–12440.

69 Barstow B, Ando N, Kim CU and Gruner SM (2008) Alteration of citrine structure by hydrostatic pressure explains the accompanying spectral shift. *Proc Natl Acad Sci U S A* **105**, 13362–13366.

70 Barstow B, Ando N, Kim CU and Gruner SM (2009) Coupling of pressure-induced structural shifts to spectral changes in a yellow fluorescent protein. *Biophys J* **97**, 1719–1727.

71 Nguyen Bich N, Moeyaert B, van Hecke K, Dedecker P, Mizuno H, Hofkens J and van Meervelt L (2012) Structural basis for the influence of a single mutation K145N on the oligomerization and photoswitching rate of Dronpa. *Acta Crystallogr D* **68**, 1653–1659.

72 Zhou XX, Chung HK, Lam AJ and Lin MZ (2012) Optical control of protein activity by fluorescent protein domains. *Science* **338**, 810–814.

73 Zhou XX, Fan LZ, Li P, Shen K and Lin MZ (2017) Optical control of cell signaling by single-chain photoswitchable kinases. *Science* **355**, 836–842.

74 Mizuno H, Dedecker P, Ando R, Fukano T, Hofkens J and Miyawaki A (2010) Higher resolution in localization microscopy by slower switching of a photochromic protein. *Photochem Photobiol Sci* **9**, 239–248.

75 Moeyaert B, Nguyen Bich N, de Zitter E, Rocha S, Clays K, Mizuno H, van Meervelt L, Hofkens J and Dedecker P (2014) Green-to-red photoconvertible Dronpa mutant for multimodal super-resolution fluorescence microscopy. *ACS Nano* **8**, 1664–1673.

76 Adam V, Lelimousin M, Boehme S, Desfonds G, Nienhaus K, Field MJ, Wiedenmann J, McSweeney S, Nienhaus GU and Bourgeois D (2008) Structural characterization of IrisFP, an optical highlighter undergoing multiple photo-induced transformations. *Proc Natl Acad Sci U S A* **105**, 18343–18348.

77 de Zitter E, Thédié D, Mönkemöller V, Hugelier S, Beaudouin J, Adam V, Byrdin M, van Meervelt L, Dedecker P and Bourgeois D (2019) Mechanistic investigation of mEos4b reveals a strategy to reduce track interruptions in sptPALM. *Nat Methods* **16**, 707–710.

78 Nienhaus K and Nienhaus GU (2021) Fluorescent proteins of the EosFP clade: intriguing marker tools with multiple photoactivation modes for advanced microscopy. *RSC Chem Biol* **2**, 796–814.

79 Zhang W, Lohman AW, Zhuravlova Y, Lu X, Wiens MD, Hoi H, Yaganoglu S, Mohr MA, Kitova EN, Klassen JS et al. (2017) Optogenetic control with a photocleavable protein, PhoCl. *Nat Methods* **14**, 391–394.

80 Greenwald EC, Mehta S and Zhang J (2018) Genetically encoded fluorescent biosensors illuminate the spatiotemporal regulation of signaling networks. *Chem Rev* **118**, 11707–11794.

81 Baird GS, Zacharias DA and Tsien RY (1999) Circular permutation and receptor insertion within green fluorescent proteins. *Proc Natl Acad Sci U S A* **96**, 11241–11246.

82 Inoue M (2021) Genetically encoded calcium indicators to probe complex brain circuit dynamics in vivo. *Neurosci Res* **169**, 2–8.

83 Patriarchi T, Cho JR, Merten K, Howe MW, Marley A, Xiong WH, Folk RW, Broussard GJ, Liang R, Jang MJ et al. (2018) Ultrafast neuronal imaging of dopamine dynamics with designed genetically encoded sensors. *Science* **360**, eaat4422.

84 Fosque BF, Sun Y, Dana H, Yang CT, Ohyama T, Tadross MR, Patel R, Zlatic M, Kim DS, Ahrens MB et al. (2015) Neural circuits. Labeling of active neural circuits in vivo with designed calcium integrators. Science 347, 755–760.

85 Moeyaert B, Holt G, Madangopal R, Perez-Alvarez A, Fearey BC, Trojanowski NF, Ledderose J, Zolnik TA, das A, Patel D et al. (2018) Improved methods for marking active neuron populations. Nat Commun 9, 4440.

86 Sha F, Abdelfattah AS, Patel R and Schreiter ER (2020) Erasable labeling of neuronal activity using a reversible calcium marker. Elife 9, 1–21.

87 Mishra K, Fuenzalida-Werner JP, Pennacchietti F, Janowski R, Chmyrov A, Huang Y, Zakian C, Klemm U, Testa I, Niessing D et al. (2022) Genetically encoded photo-switchable molecular sensors for optoacoustic and super-resolution imaging. Nat Biotechnol 40, 598–605.

88 Bierbuesse F, Bourges AC, Gielen V, Mönkemöller V, Vandenberg W, Shen Y, Hofkens J, Vanden Berghe P, Campbell RE, Moeyaert B et al. (2022) Absolute measurement of cellular activities using photochromic single-fluorophore biosensors and intermittent quantification. Nat Commun 13, 1850.

89 Helassa N, Podor B, Fine A and Török K (2016) Design and mechanistic insight into ultrafast calcium indicators for monitoring intracellular calcium dynamics. Sci Rep 6, 1–14.

90 Helassa N, Zhang XH, Conte I, Scaringi J, Esposito E, Bradley J, Carter T, Ogden D, Morad M and Török K (2015) Fast-response calmodulin-based fluorescent indicators reveal rapid intracellular calcium dynamics. Sci Rep 5, 15978.

91 Adelizzi B, Gielen V, le Saux T, Dedecker P and Jullien L (2021) Quantitative model for reversibly photoswitchable sensors. ACS Sens 6, 1157–1165.

92 Marvin JS, Borghuis BG, Tian L, Cichon J, Harnett MT, Akerboom J, Gordus A, Renninger SL, Chen TW, Bargmann CI et al. (2013) An optimized fluorescent probe for visualizing glutamate neurotransmission. Nat Methods 10, 162–170.

93 Qian Y, Piatkevich KD, Mc Larney B, Abdelfattah AS, Mehta S, Murdock MH, Gottschalk S, Molina RS, Zhang W, Chen Y et al. (2019) A genetically encoded near-infrared fluorescent calcium ion indicator. Nat Methods 16, 171–174.

94 Subach OM, Barykina N v, Anokhin K v, Piatkevich KD and Subach FV (2019) Near-infrared genetically encoded positive calcium indicator based on gaf-fp bacterial phytochrome. Int J Mol Sci 20, 3488.

95 Rockwell NC and Lagarias JC (2010) A brief history of phytochromes. ChemPhysChem 11, 1172–1180.

96 Lu X, Shen Y and Campbell RE (2020) Engineering photosensory modules of non-opsin-based optogenetic actuators. Int J Mol Sci 21, 1–25.

97 Shcherbakova DM, Baloban M and Verkhusha VV (2015) Near-infrared fluorescent proteins engineered from bacterial phytochromes. Curr Opin Chem Biol 27, 52–63.

98 Wiltbank LB and Kehoe DM (2019) Diverse light responses of cyanobacteria mediated by phytochrome superfamily photoreceptors. Nat Rev Microbiol 17, 37–50.

99 Cheng M-C, Kathare PK, Paik I and Huq E (2021) Phytochrome signaling networks. Annu Rev Plant Biol 72, 217–244.

100 Auldridge ME and Forest KT (2011) Bacterial phytochromes: more than meets the light. Crit Rev Biochem Mol Biol 46, 67–88.

101 Maines MD (1988) Heme oxygenase: function, multiplicity, regulatory mechanisms, and clinical applications. FASEB J 2, 2557–2568.

102 Wagner JR, Brunzelle JS, Forest KT and Vierstra RD (2005) A light-sensing knot revealed by the structure of the chromophore-binding domain of phytochrome. Nature 438, 325–331.

103 Lamparter T, Carrascal M, Michael N, Martinez E, Rottwinkel G and Abian J (2004) The biliverdin chromophore binds covalently to a conserved cysteine residue in the N-terminus of Agrobacterium phytochrome Agp1. Biochemistry 43, 3659–3669.

104 Rottwinkel G, Oberpichler I and Lamparter T (2010) Bathy phytochromes in rhizobial soil bacteria. J Bacteriol 192, 5124–5133.

105 Giraud E and Verméglio A (2008) Bacteriophytochromes in anoxygenic photosynthetic bacteria. Photosynth Res 97, 141–153.

106 Takala H, Edlund P, Ihalainen JA and Westenhoff S (2020) Tips and turns of bacteriophytochrome photoactivation. Photochem Photobiol Sci 19, 1488.

107 Yang X, Ren Z, Kuk J and Moffat K (2011) Temperature-scan cryocrystallography reveals reaction intermediates in bacteriophytochrome. Nature 479, 428–431.

108 Toh KC, Stojkovic EA, van Stokkum IHM, Moffat K and Kennis JTM (2010) Proton-transfer and hydrogen-bond interactions determine fluorescence quantum yield and photochemical efficiency of bacteriophytochrome. Proc Natl Acad Sci U S A 107, 9170–9175.

109 Andel F, Hasson KC, Gai F, Anfinrud PA and Mathies RA (1997) Femtosecond time-resolved spectroscopy of the primary photochemistry of phytochrome. Biospectroscopy 3, 421–433.

110 Mroginski MA, Murgida DH and Hildebrandt P (2007) The chromophore structural changes during the photocycle of phytochrome: a combined resonance Raman and quantum chemical approach. Acc Chem Res 40, 258–266.

111 van Thor JJ, Ronayne KL and Towrie M (2007) Formation of the early photoproduct Lumi-R of

cyanobacterial phytochrome Cph1 observed by ultrafast mid-infrared spectroscopy. *J Am Chem Soc* **129**, 126–132.

112 Dasgupta J, Frontiera RR, Taylor KC, Lagarias JC and Mathies RA (2009) Ultrafast excited-state isomerization in phytochrome revealed by femtosecond stimulated Raman spectroscopy. *Proc Natl Acad Sci U S A* **106**, 1784–1789.

113 Salvadori G, Macaluso V, Pellicci G, Cupellini L, Granucci G and Mennucci B (2022) Protein control of photochemistry and transient intermediates in phytochromes. *Nat Commun* **13**, 6838.

114 Claesson E, Wahlgren WY, Takala H, Pandey S, Castillon L, Kuznetsova V, Henry L, Panman M, Carrillo M, Kübel J *et al.* (2020) The primary structural photoresponse of phytochrome proteins captured by a femtosecond X-ray laser. *Elife* **9**, e53514.

115 Mathes T, Ravensbergen J, Kloz M, Gleichmann T, Gallagher KD, Woitowich NC, St. Peter R, Kovaleva SE, Stojković EA and Kennis JTM (2015) Femto- to microsecond photodynamics of an unusual bacteriophytochrome. *J Phys Chem Lett* **6**, 239–243.

116 Borucki B, von Stetten D, Seibeck S, Lamparter T, Michael N, Mroginski MA, Otto H, Murgida DH, Heyn MP and Hildebrandt P (2005) Light-induced proton release of phytochrome is coupled to the transient deprotonation of the tetrapyrrole chromophore. *J Biol Chem* **280**, 34358–34364.

117 Velazquez Escobar F, Piwowarski P, Salewski J, Michael N, Fernandez Lopez M, Rupp A, Qureshi BM, Scheerer P, Bartl F, Frankenberg-Dinkel N *et al.* (2015) A protonation-coupled feedback mechanism controls the signalling process in bathy phytochromes. *Nat Chem* **7**, 423–430.

118 Rohmer T, Lang C, Bongards C, Gupta KBSS, Neugebauer J, Hughes J, Gärtner W and Matysik J (2010) Phytochrome as molecular machine: revealing chromophore action during the Pfr → Pr photoconversion by magic-angle spinning NMR spectroscopy. *J Am Chem Soc* **132**, 4431–4437.

119 Eilfeld P and Rüdiger W (1985) Absorption spectra of phytochrome intermediates. *Z Naturforsch C* **40**, 109–114.

120 Schumann C, Groß R, Wolf MMN, Diller R, Michael N and Lamparter T (2008) Subpicosecond midinfrared spectroscopy of the Pfr reaction of phytochrome Agp1 from *Agrobacterium tumefaciens*. *Biophys J* **94**, 3189–3197.

121 Consiglieri E, Gutt A, Gärtner W, Schubert L, Viappiani C, Abbruzzetti S and Losi A (2019) Dynamics and efficiency of photoswitching in biliverdin-binding phytochromes. *Photochem Photobiol Sci* **18**, 2484–2496.

122 Klose C, Nagy F and Schäfer E (2020) Thermal reversion of plant phytochromes. *Mol Plant* **13**, 386–397.

123 Zienicke B, Molina I, Glenz R, Singer P, Ehmer D, Escobar FV, Hildebrandt P, Diller R and Lamparter T (2013) Unusual spectral properties of bacteriophytochrome Agp2 result from a deprotonation of the chromophore in the red-absorbing form Pr. *J Biol Chem* **288**, 31738–31751.

124 Yu Z, Ali A, Igbalajobi OA, Streng C, Leister K, Krauß N, Lamparter T and Fischer R (2019) Two hybrid histidine kinases, TcsB and the phytochrome FphA, are involved in temperature sensing in *Aspergillus nidulans*. *Mol Microbiol* **112**, 1814–1830.

125 Merga G, Lopez MF, Fischer P, Piwowarski P, Nogacz Ż, Kraskov A, Buhrke D, Escobar FV, Michael N, Siebert F *et al.* (2021) Light- and temperature-dependent dynamics of chromophore and protein structural changes in bathy phytochrome Agp2. *Phys Chem Chem Phys* **23**, 18197–18205.

126 Davis SJ, Vener AV and Vierstra RD (1999) Bacteriophytochromes: phytochrome-like photoreceptors from nonphotosynthetic eubacteria. *Science* **286**, 2517–2520.

127 Edlund P, Takala H, Claesson E, Henry L, Dods R, Lehtivuori H, Panman M, Pande K, White T, Nakane T *et al.* (2016) The room temperature crystal structure of a bacterial phytochrome determined by serial femtosecond crystallography. *Sci Rep* **6**, 35279.

128 Burgie ES, Wang T, Bussell AN, Walker JM, Li H and Vierstra RD (2014) Crystallographic and electron microscopic analyses of a bacterial phytochrome reveal local and global rearrangements during photoconversion. *J Biol Chem* **289**, 24573–24587.

129 Song C, Psakis G, Lang C, Mailliet J, Gärtner W, Hughes J and Matysik J (2011) Two ground state isoforms and a chromophore D-ring photoflip triggering extensive intramolecular changes in a canonical phytochrome. *Proc Natl Acad Sci U S A* **108**, 3842–3847.

130 Lenngren N, Edlund P, Takala H, Stucki-Buchli B, Rumfeldt J, Peshev I, Häkkänen H, Westenhoff S and Ihalainen JA (2018) Coordination of the biliverdin D-ring in bacteriophytochromes. *Phys Chem Chem Phys* **20**, 18216–18225.

131 Essen L-O, Mailliet J and Hughes J (2008) The structure of a complete phytochrome sensory module in the Pr ground state. *Proc Natl Acad Sci* **105**, 14709–14714.

132 Yang X, Kuk J and Moffat K (2008) Crystal structure of *Pseudomonas aeruginosa* bacteriophytochrome: photoconversion and signal transduction. *Proc Natl Acad Sci U S A* **105**, 14715–14720.

133 Takala H, Lehtivuori H, Hammarén H, Hytönen VP and Ihalainen JA (2014) Connection between absorption properties and conformational changes in *Deinococcus radiodurans* phytochrome. *Biochemistry* **53**, 7076–7085.

134 Nagano S, Scheerer P, Zubow K, Michael N, Inomata K, Lamparter T and Krauß N (2016) The crystal structures of the N-terminal photosensory core module of agrobacterium phytochrome Agp1 as parallel and anti-parallel dimers. *J Biol Chem* **291**, 20674–20691.

135 Yang X, Stojković EA, Ozarowski WB, Kuk J, Davydova E and Moffat K (2015) Light signaling mechanism of two tandem bacteriophytochromes. *Structure* **23**, 1179–1189.

136 Burgie ES, Zhang J and Vierstra RD (2016) Crystal structure of Deinococcus phytochrome in the photoactivated state reveals a cascade of structural rearrangements during Photoconversion. *Structure* **24**, 448–457.

137 Karniol B and Vierstra RD (2003) The pair of bacteriophytochromes from *Agrobacterium tumefaciens* are histidine kinases with opposing photobiological properties. *Proc Natl Acad Sci* **100**, 2807–2812.

138 Giraud E, Hannibal L, Fardoux J, Jaubert M, Jourand P, Dreyfus B, Sturgis JN and Verméglio A (2004) Two distinct crt gene clusters for two different functional classes of carotenoid in *Bradyrhizobium*. *J Biol Chem* **279**, 15076–15083.

139 Papiz MZ, Bellini D, Evans K, Grossmann JG and Fordham-Skelton T (2019) Light-induced complex formation of bacteriophytochrome RpBphP1 and gene repressor RpPpsR2 probed by SAXS. *FEBS J* **286**, 4261–4277.

140 Giraud E, Zappa S, Vuillet L, Adriano JM, Hannibal L, Fardoux J, Berthomieu C, Bouyer P, Pignol D and Verméglio A (2005) A new type of bacteriophytochrome acts in tandem with a classical bacteriophytochrome to control the antennae synthesis in *Rhodopseudomonas palustris*. *J Biol Chem* **280**, 32389–32397.

141 Björling A, Berntsson O, Lehtivuori H, Takala H, Hughes AJ, Panman M, Hoernke M, Niebling S, Henry L, Henning R *et al.* (2016) Structural photoactivation of a full-length bacterial phytochrome. *Sci Adv* **2**, e1600920.

142 Otero LH, Klinke S, Rinaldi J, Velázquez-Escobar F, Mroginski MA, Fernández López M, Malamud F, Vojnov AA, Hildebrandt P, Goldbaum FA *et al.* (2016) Structure of the full-length bacteriophytochrome from the plant pathogen *Xanthomonas campestris* provides clues to its long-range signaling mechanism. *J Mol Biol* **428**, 3702–3720.

143 Gourinchas G, Etzl S, Göbl C, Vide U, Madl T and Winkler A (2017) Long-range allosteric signaling in red light-regulated diguanylyl cyclases. *Sci Adv* **3**, e1602498.

144 Gourinchas G, Heintz U and Winkler A (2018) Asymmetric activation mechanism of a homodimeric red light-regulated photoreceptor. *Elife* **7**, e34815.

145 Berntsson O, Diensthuber RP, Panman MR, Björling A, Gustavsson E, Hoernke M, Hughes AJ, Henry L, Niebling S, Takala H *et al.* (2017) Sequential conformational transitions and α-helical supercoiling regulate a sensor histidine kinase. *Nat Commun* **8**, 284.

146 Gushchin I, Melnikov I, Polovinkin V, Ishchenko A, Yuzhakova A, Buslaev P, Bourenkov G, Grudinin S, Round E, Balandin T *et al.* (2017) Mechanism of transmembrane signaling by sensor histidine kinases. *Science* **356**, eaah6345.

147 Etzl S, Lindner R, Nelson MD and Winkler A (2018) Structure-guided design and functional characterization of an artificial red light–regulated guanylate/adenylate cyclase for optogenetic applications. *J Biol Chem* **293**, 9078–9089.

148 Wahlgren WY, Claesson E, Tuure I, Trillo-Muyo S, Bódizs S, Ihalainen JA, Takala H and Westenhoff S (2022) Structural mechanism of signal transduction in a phytochrome histidine kinase. *Nat Commun* **13**, 7673.

149 Bhate MP, Molnar KS, Goulian M and DeGrado WF (2015) Signal transduction in histidine kinases: insights from new structures. *Structure* **23**, 981–994.

150 Möglich A (2019) Signal transduction in photoreceptor histidine kinases. *Protein Sci* **28**, 1923–1946.

151 Takala H, Niebling S, Berntsson O, Björling A, Lehtivuori H, Häkkänen H, Panman M, Gustavsson E, Hoernke M, Newby G *et al.* (2016) Light-induced structural changes in a monomeric bacteriophytochrome. *Struct Dyn* **3**, 054701.

152 De N, Navarro MVAS, Raghavan RV and Sondermann H (2009) Determinants for the activation and autoinhibition of the diguanylate cyclase response regulator WspR. *J Mol Biol* **393**, 619–633.

153 Schirmer T and Jenal U (2009) Structural and mechanistic determinants of c-di-GMP signalling. *Nat Rev Microbiol* **7**, 724–735.

154 Takala H, Björling A, Berntsson O, Lehtivuori H, Niebling S, Hoernke M, Kosheleva I, Henning R, Menzel A, Ihalainen JA *et al.* (2014) Signal amplification and transduction in phytochrome photosensors. *Nature* **509**, 245–248.

155 Li H, Zhang J, Vierstra RD and Li H (2010) Quaternary organization of a phytochrome dimer as revealed by cryoelectron microscopy. *Proc Natl Acad Sci* **107**, 10872–10877.

156 Bellini D and Papiz MZ (2012) Structure of a bacteriophytochrome and light-stimulated protomer swapping with a gene repressor. *Structure* **20**, 1436–1446.

157 Otero LH, Foscaldi S, Antelo GT, Rosano GL, Sirigu S, Klinke S, Defelipe LA, Sánchez-Lamas M, Battocchio G, Conforte V *et al.* (2021) Structural basis for the Pr-Pfr long-range signaling mechanism of a

full-length bacterial phytochrome at the atomic level. *Sci Adv* **7**, 1097.

158 Ryu M-H, Kang IH, Nelson MD, Jensen TM, Lyuksyutova AI, Siltberg-Liberles J, Raizen DM and Gomelsky M (2014) Engineering adenylate cyclases regulated by near-infrared window light. *Proc Natl Acad Sci U S A* **111**, 10167–10172.

159 Takala H, Lehtivuori HK, Berntsson O, Hughes A, Nanekar R, Niebling S, Panman M, Henry L, Menzel A, Westenhoff S et al. (2018) On the (un)coupling of the chromophore, tongue interactions, and overall conformation in a bacterial phytochrome. *J Biol Chem* **293**, 8161–8172.

160 Gourinchas G, Vide U and Winkler A (2019) Influence of the N-terminal segment and the PHY-tongue element on light-regulation in bacteriophytochromes. *J Biol Chem* **294**, 4498–4510.

161 Shcherbakova DM, Stepanenko OV, Turoverov KK and Verkhusha VV (2018) Near-infrared fluorescent proteins: multiplexing and optogenetics across scales HHS public access. *Trends Biotechnol* **36**, 1230–1243.

162 Ryu M-H and Gomelsky M (2014) Near-infrared light responsive synthetic c-di-GMP module for optogenetic applications. *ACS Synth Biol* **3**, 802–810.

163 Gasser C, Taiber S, Yeh CM, Wittig CH, Hegemann P, Ryu S, Wunder F and Möglich A (2014) Engineering of a red-light–activated human cAMP/cGMP-specific phosphodiesterase. *Proc Natl Acad Sci* **111**, 8803–8808.

164 Leopold, A. V., Pletnev, S. & Verkhusha, V. v. Bacterial phytochrome as a scaffold for engineering of receptor tyrosine kinases controlled with near-infrared light. *J Mol Biol* **432**, 3749–3760 (2020).

165 Kaberniuk A, Shemetov AA and Verkhusha VV (2016) A bacterial phytochrome-based optogenetic system controllable with near-infrared light. *Nat Methods* **13**, 591–597.

166 Rumyantsev KA, Shcherbakova DM, Zakharova NI, Emelyanov AV, Turoverov KK and Verkhusha VV (2015) Minimal domain of bacterial phytochrome required for chromophore binding and fluorescence. *Sci Rep* **5**, 18348.

167 Shcherbakova DM, Stepanenko OV, Turoverov KK and Verkhusha VV (2018) Near-infrared fluorescent proteins: multiplexing and optogenetics across scales. *Trends Biotechnol* **36**, 1230–1243.

168 Shcherbakova DM, Baloban M, Emelyanov AV, Brenowitz M, Guo P and Verkhusha VV (2016) Bright monomeric near-infrared fluorescent proteins as tags and biosensors for multiscale imaging. *Nat Commun* **7**, 12405.

169 Matlashov ME, Shcherbakova DM, Alvelid J, Baloban M, Pennacchietti F, Shemetov AA, Testa I and Verkhusha VV (2020) A set of monomeric near-infrared fluorescent proteins for multicolor imaging across scales. *Nat Commun* **11**, 239.

170 Karlas A, Pleitez MA, Aguirre J and Ntziachristos V (2021) Optoacoustic imaging in endocrinology and metabolism. *Nat Rev Endocrinol* **17**, 323–335.

171 Omar M, Aguirre J and Ntziachristos V (2019) Optoacoustic mesoscopy for biomedicine. *Nat Biomed Eng* **3**, 354–370.

172 Yao J and Wang LV (2018) Recent progress in photoacoustic molecular imaging. *Curr Opin Chem Biol* **45**, 104–112.

173 Lin L and Wang LV (2022) The emerging role of photoacoustic imaging in clinical oncology. *Nat Rev Clin Oncol* **19**, 365–384.

174 Yao J, Kaberniuk AA, Li L, Shcherbakova DM, Zhang R, Wang L, Li G, Verkhusha VV and Wang LV (2015) Multiscale photoacoustic tomography using reversibly switchable bacterial phytochrome as a near-infrared photochromic probe. *Nat Methods* **13**, 67–73.

175 Chee RKW, Li Y, Zhang W, Campbell RE and Zemp RJ (2018) In vivo photoacoustic difference-spectra imaging of bacteria using photoswitchable chromoproteins. *J Biomed Opt* **23**, 1–11.

176 Gao R, Liu F, Liu W, Zeng S, Chen J, Gao R, Wang L, Fang C, Song L, Sedgwick AC et al. (2022) Background-suppressed tumor-targeted photoacoustic imaging using bacterial carriers. *Proc Natl Acad Sci U S A* **119**, e2121982119.

177 Mishra K, Stankevych M, Fuenzalida-Werner JP, Grassmann S, Gujrati V, Huang Y, Klemm U, Buchholz VR, Ntziachristos V and Stiel AC (2020) Multiplexed whole-animal imaging with reversibly switchable optoacoustic proteins. *Sci Adv* **6**, eaaz6293.

178 Li L, Shemetov AA, Baloban M, Hu P, Zhu L, Shcherbakova DM, Zhang R, Shi J, Yao J, Wang LV et al. (2018) Small near-infrared photochromic protein for photoacoustic multi-contrast imaging and detection of protein interactions in vivo. *Nat Commun* **9**, 2734.

179 Kasatkina LA, Ma C, Matlashov ME, Vu T, Li M, Kaberniuk AA, Yao J and Verkhusha VV (2022) Optogenetic manipulation and photoacoustic imaging using a near-infrared transgenic mouse model. *Nat Commun* **13**, 2813.

180 Shcherbakova DM, Cox Cammer N, Huisman TM, Verkhusha VV and Hodgson L (2018) Direct multiplex imaging and optogenetics of Rho GTPases enabled by near-infrared FRET. *Nat Chem Biol* **14**, 591–600.

181 Shemetov AA, Monakhov MV, Zhang Q, Canton-Josh JE, Kumar M, Chen M, Matlashov ME, Li X, Yang W, Nie L et al. (2021) A near-infrared genetically encoded calcium indicator for in vivo imaging. *Nat Biotechnol* **39**, 368–377.

182 Pandey N, Kuypers BE, Nassif B, Thomas EE, Alnahhas RN, Segatori L and Silberg JJ (2016)

Tolerance of a knotted near-infrared fluorescent protein to random circular permutation. *Biochemistry* **55**, 3763–3773.

183 Qian Y, Cosio DMO, Piatkevich KD, Aufmkolk S, Su WC, Celiker OT, Schohl A, Murdock MH, Aggarwal A, Chang YF *et al.* (2020) Improved genetically encoded near-infrared fluorescent calcium ion indicators for in vivo imaging. *PLoS Biol* **18**, e3000965.

184 Hashizume R, Fujii H, Mehta S, Ota K, Qian Y, Zhu W, Drobizhev M, Nasu Y, Zhang J, Bito H *et al.* (2022) A genetically encoded far-red fluorescent calcium ion biosensor derived from a biliverdin-binding protein. *Protein Sci* **31**, e4440.

185 Subach OM and Subach FV (2020) GAF-CaMP3-sfGFP, an enhanced version of the near-infrared genetically encoded positive phytochrome-based calcium indicator for the visualization of neuronal activity. *Int J Mol Sci* **21**, 6883.

Supporting information

Additional supporting information may be found online in the Supporting Information section at the end of the article.

Table S1. Basic information on proteins discussed in this review.
Table S2. Photoswitched structures of RSFPs.
Table S3. Overview of BphP structures.
Figure S1. Photophysical states and chromophore conformation of rsEGFP2.